UC San Diego

UC San Diego Previously Published Works

Title

Inherited chitinases enable sustained growth and rapid dispersal of bacteria from chitin particles

Permalink

Journal

ISSN

Authors

Guessous, Ghita
Patsalo, Vadim
Balakrishnan, Rohan
et al.

Publication Date

DOI

Copyright Information

Peer reviewed

Article

Inherited chitinases enable sustained growth and rapid dispersal of bacteria from chitin particles

Check for updates

Ghita Guessous [1], Vadim Patsalo [2,3], Rohan Balakrishnan [1], Tolga Çağlar[1,4], James R. Williamson [2] & Terence Hwa [1]

Many biogeochemical functions involve bacteria utilizing solid substrates. However, little is known about the coordination of bacterial growth with the kinetics of attachment to and detachment from such substrates. In this quantitative study of *Vibrio* sp. 1A01 growing on chitin particles, we reveal the heterogeneous nature of the exponentially growing culture comprising two co-existing subpopulations: a minority replicating on chitin particles and a non-replicating majority which was planktonic. This partition resulted from a high rate of cell detachment from particles. Despite high detachment, sustained exponential growth of cells on particles was enabled by the enrichment of extracellular chitinases excreted and left behind by detached cells. The 'inheritance' of these chitinases sustains the colonizing subpopulation despite its reduced density. This simple mechanism helps to circumvent a trade-off between growth and dispersal, allowing particle-associated marine heterotrophs to explore new habitats without compromising their fitness on the habitat they have already colonized.

While bacterial growth in homogeneous environments has been well characterized[1], much less is known about growth on solid substrates. Unlike in liquid cultures where nutrients are homogeneously distributed and the population increases exponentially, the temporal characteristics of populations growing in heterogeneous cultures can vary substantially depending on the structure of the environment. This is because temporal and spatial differences in nutrient concentrations may result in the emergence of subpopulations, each adapting to their local environments[2].

Also, growth on solid substrates complicates our understanding of population fitness, as individuals must not only consume their current substrate to replicate, but must also successfully seed new habitats to grow further. This tension between growth on the current resource and dispersal from it to find new habitats is at the heart of the colonization–dispersal trade-off[3–5].

While seemingly homogeneous, the ocean offers a highly structured nutrient landscape at the microscopic scale[6–8]. Faecal pellets,

organic detritus and dead carcasses (generally termed marine snow)[9,10] constitute a large pool of resources that heterotrophic bacteria can utilize as a source of nutrients and energy. One of the major constituents of marine snow is chitin[11,12], a biopolymer of GlcNAc molecules that is highly insoluble in water[13,14]. Chitin is degraded by heterotrophic bacteria such as *Vibrios*[15–18], which express hydrolytic enzymes called chitinases to break down the long polymeric chains into labile nutrients[19,20]. This makes chitin a favourable candidate for studying bacterial strategies for utilization of particulate substrates.

Previous studies have characterized isolated components of bacteria–chitin interactions, including enzyme kinetics[19,21–23], cell replication[16,17], cell attachment[24–26] and detachment dynamics[27] as well as motility[28,29]. However, as we will show, growth on chitin is highly dynamic, involving the simultaneous interaction of these processes. It is thus crucial to integrate these components for the same cells and conditions to build a comprehensive understanding of chitin degradation

[1]Department of Physics, University of California at San Diego, La Jolla, CA, USA. [2]Department of Integrative Structural and Computational Biology, and The Skaggs Institute for Chemical Biology, The Scripps Research Institute, La Jolla, CA, USA. [3]Present address: DataBricks, San Diego, CA, USA. [4]Present address: San Diego Supercomputer Center, La Jolla, CA, USA. ✉e-mail: hwa@ucsd.edu
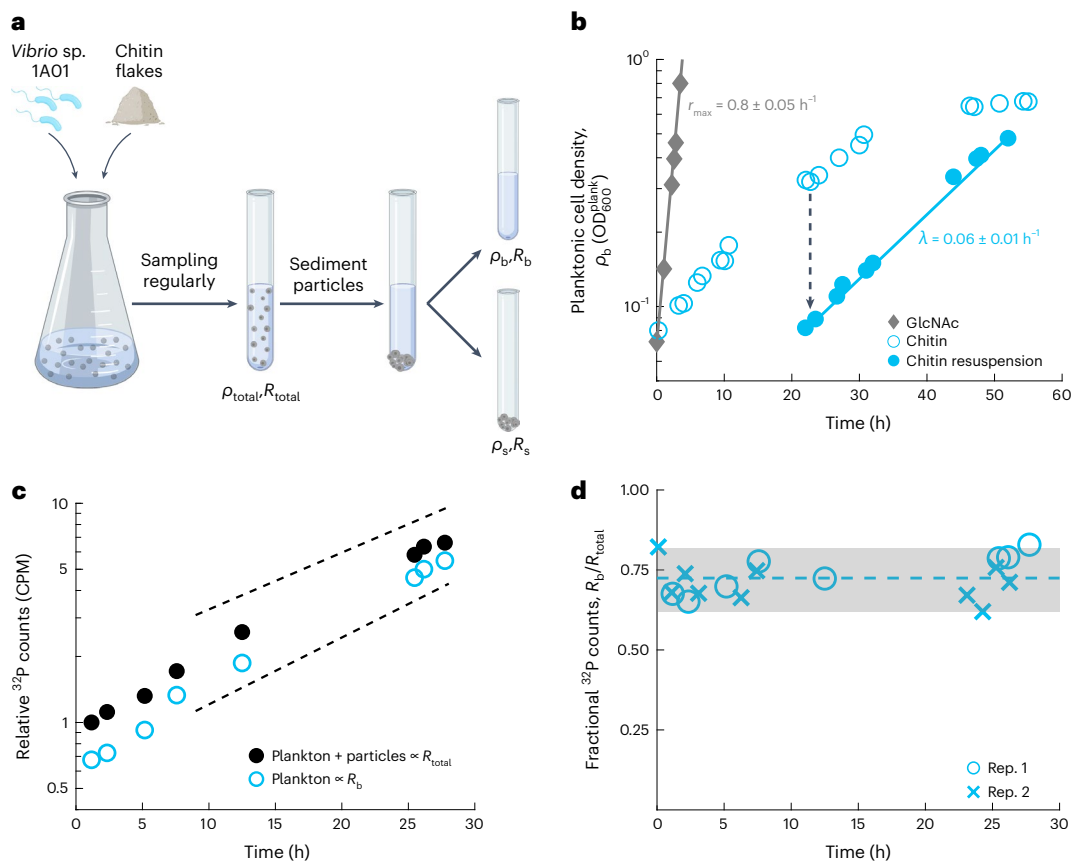
Fig. 1 | Steady-state growth of two subpopulations on chitin particles.
a, *Vibrio* sp. 1A01 cells were grown with chitin flakes as the sole carbon and nitrogen source. The culture was periodically sampled for measurements. For each sample, the culture was fractionated by sedimenting the chitin flakes and separating them from the planktonic component. Measurements of the planktonic fraction yielded the planktonic cell density (ρ_b, **b**) and planktonic RNA content (R_b, **c**). Measurements of the full culture yielded the total RNA content (R_{total}, **c**), and hence the ratio (R_b:R_{total}, **d**). **b**, Open blue circles represent OD_{600} readings of the planktonic fraction of the chitin culture at various times after inoculation. At 24 h after inoculation, the planktonic component of this culture was used to inoculate a fresh chitin culture (dashed arrow). Subsequent OD_{600} measurements are shown as the filled blue circles. The data indicate exponential increase of the planktonic component of the culture at a rate $\lambda = 0.06 \pm 0.01\ h^{-1}$ (solid blue line). For comparison, growth of 1A01 on GlcNAc (grey diamonds) exhibits -13× faster growth rate (solid grey line). Population increase rates were determined by fitting an exponential model; the error is the standard deviation

across 6 biological replicates. **c**, ^{32}P was used to label the cells' RNA (Methods) in a chitin culture and radioactivity was tracked in samples of the full culture (R_{total}, filled black circles) as well as in planktonic samples (R_b, open blue circles). Radioactivity increased exponentially and at approximately the same rate in both. The upper and lower dashed lines represent population increase rates of $\lambda = 0.06\ h^{-1}$ and $\lambda = 0.07\ h^{-1}$, respectively, and are provided as a guide. **d**, Open blue circles represent the ratio in signal between the two samples in **c**, R_b:R_{total}, and blue crosses are results from a replicate. The grey area spans the range of our data between the minimum and maximum estimate. We find R_b:$R_{total} \approx 0.72 \pm 0.06$ where the error is the standard deviation across all samples. This ratio allows us to deduce the fraction of RNA from particle-associated cells, R_s:R_{total}, which is corroborated by direct measurement (Extended Data Fig. 1c,d). After adjusting for the cellular RNA amount in each fraction (R_b:ρ_b and R_s:ρ_s) as described in Extended Data Fig. 1b, the ratio of planktonic cells in the culture is deduced: ρ_b:$\rho_{total} \approx 0.75 \pm 0.06$.

that bridges cellular descriptions to population-level ones. Such a picture would contribute to informing macroscopic models of carbon cycling[2] and constraining bacterial contributions therein.

In our study, we characterized the space-dependent growth and dispersal of a natural chitinolytic isolate, *Vibrio* sp. 1A01 (refs. 26–28), which can utilize chitin particles as its sole source of carbon and nitrogen. Despite the heterogeneous environment, the culture exhibited exponential dynamics, with two subpopulations arising: a replicating minority on the particles and a majority of non-replicating cells, continuously detaching from chitin. We uncovered a population-level scheme involving the use of secreted chitinases, which enabled the particle-associated minority to replicate sufficiently rapidly to drive the exponential increase of both subpopulations. This unexpected behaviour is interpreted in light of the marine context in which cells must continuously colonize fresh particles to survive. It provides a novel mechanism through which bacterial populations can circumvent the colonization–dispersal trade-off.

Results

Steady-state growth with two co-existing subpopulations

Vibrio splendidus 1A01 was isolated from a natural community of marine bacteria[30]. When incubated in a minimal medium with chitin flakes as the sole source of carbon and nitrogen, the planktonic component of the culture (Fig. 1a) increased exponentially at a rate $\lambda \approx 0.06 \pm 0.01\ h^{-1}$ (-12 h per doubling; open blue circles Fig. 1b). Upon transferring the planktonic component to a fresh medium with fresh chitin particles, the exponential increase resumed at the same rate (solid circles, Fig. 1b). In comparison, growth was much faster ($r_{max} = 0.8 \pm 0.05\ h^{-1}$, -1 h per doubling) on GlcNAc, the monomer of chitin (diamonds, Fig. 1b), suggesting additional bottleneck(s) related to chitin utilization.

To observe growth of cells on particles, we measured the incorporation of radioactive tracers in biomass: we monitored the incorporation of ^{32}P in cells collected from the entire culture, R_{total} (filled circles in Fig. 1c), and from the planktonic component, R_b (open circles). Radioactivity increased at the same exponential rate for both

populations (Fig. 1c), similarly to the rate of planktonic optical density (OD) increase (Fig. 1b). These results establish the co-existence of two exponentially increasing subpopulations: one in the planktonic or **b**ulk state, ρ_b, and the other on the **s**urface of chitin particles, ρ_s. The ratio of radioactive signals in the two samples, R_b:R_{total} (Fig. 1d), together with the RNA contents of the subpopulations R_b/ρ_b and R_s/ρ_s (Extended Data Fig. 1a,b), allowed us to estimate the relative abundance of each subpopulation, with ρ_b:$\rho_{total} \approx 0.75 \pm 0.06$, which was maintained throughout the culture's growth (Fig. 1d). This is further corroborated by direct measurements of total RNA amounts in each subpopulation (Extended Data Fig. 1c), which yielded an abundance ratio ρ_b:$\rho_{total} \approx 0.8 \pm 0.1$ (Extended Data Fig. 1d). Thus, while both subpopulations increased exponentially, the majority (75–80%) of the cells were in the planktonic phase. Is the exponential increase in the planktonic fraction due to cellular replication or to the detachment of cells from particles?

Planktonic cells do not replicate despite density increase

This increase of the planktonic biomass was surprising since chitin particles are the only source of nutrients in the culture. A possible explanation is that dissolved nutrients such as GlcNAc, generated by surface-associated cells could leak into the medium supporting the replication of planktonic cells. Model calculations taking into account GlcNAc generation on the surface, its uptake and diffusion indicate that this scenario is unlikely beyond a small 'screening distance' around the particles for the observed range of cell densities (Supplementary Note III-1). Moreover, according to our model, this 'screening distance' which depends on the particle density exponentially decreases, localizing the nutrients to the surface of the particle. Consequently, planktonic cells are highly delocalized and can be treated as effectively being at constant density away from the particles (Supplementary Note III-2). Below, we describe a series of experiments establishing the lack of replication of planktonic cells.

First, analysing the composition of the supernatant by high-performance liquid chromatography (HPLC) shows that the concentrations of expected nutrients such as GlcNAc, short GlcNAc oligomers and acetate are all below our detection limit (Extended Data Fig. 2a). Although low concentrations of dissolved nutrients do not necessarily indicate the lack of cellular replication due to possibly high affinities of *Vibrio* for these substrates, we also found that the supernatant alone does not support the growth of planktonic cells (open diamonds in Fig. 2b).

The absence of growth on the supernatant only may be due to the lack of a low but steady supply of dissolved nutrients resulting from chitinolytic activity on the surface. To replicate the situation in our culture, we physically separated planktonic cells from the particles using a dialysis bag (Fig. 2c). While the dialysis bag prevents particles and cells from exchanging, it allows small molecules such as GlcNAc to permeate its membrane (Extended Data Fig. 2b). Tracking the OD of the planktonic component outside the dialysis bag shows that it did not increase (Fig. 2d), indicating a lack of cellular replication.

Finally, we directly characterized the metabolic activity of the planktonic and particle-associated subpopulations by quantifying their respective RNA synthesis rates. We found that the rate of incorporation of ^{3}H-uridine was 12 times faster in the presence of particles (Extended Data Fig. 3), even though they contained only 1/4 of the biomass (Fig. 1d). This suggests that the replication rate of planktonic cells is ~1/50 of that of cells on particles. Taken together, these experiments indicate that the exponential increase in the density of planktonic cells is not a result of cellular replication.

Cell shedding from particles supplies the planktonic population

We hypothesize that instead, the observed increase is due to the shedding of cells from particles. Inspecting the culture under a confocal microscope, we found that while chitin particles were only loosely occupied by cells and their surface area was not limiting (Extended Data
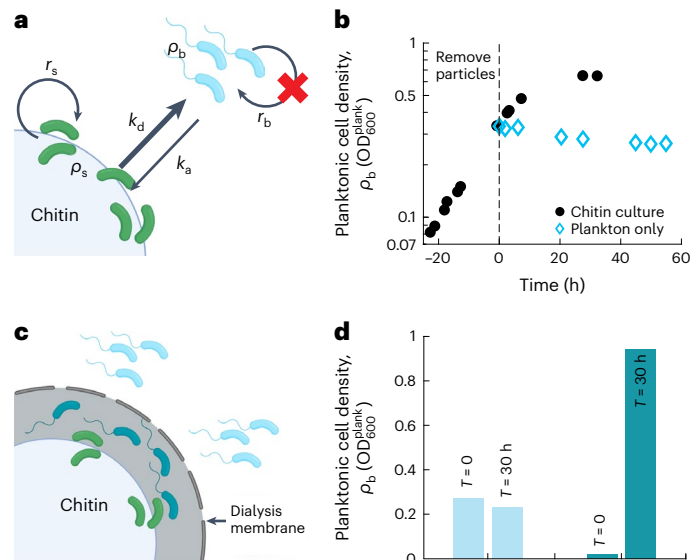

Fig. 2 | Planktonic cells are not replicating. a, A simple population model for the chitin culture: planktonic and particle-associated cells, with cell densities ρ_b and ρ_s, respectively, replicate with respective rates r_b and r_s, and exchange with an attachment rate k_a and a detachment rate k_d. Both subpopulations increase exponentially and at the same steady-state rate λ. The experiments in **b** and **d** along with that in Extended Data Fig. 3 lead to the estimate $r_b \approx 0$ (red cross). **b**, Chitin particles were removed from an exponentially increasing chitin culture (black circles) at time 0 (dashed line), and OD$_{600}$ of the remaining planktonic fraction was tracked (blue diamonds). The OD of the planktonic fraction did not increase in 60 h, indicating that growth of the planktonic cells cannot be sustained without the chitin particles. **c**, From an exponentially increasing chitin culture, chitin particles colonized with cells (green cells) were placed inside a dialysis bag (grey outline) with a 14 kDa molecular weight cut-off, while planktonic cells (blue cells) were left outside the bag. The pore size allows for small molecules such as GlcNAc to permeate but not enzymes, cells or chitin particles. Newly released cells from the surface of particles inside the bag are represented by the teal cells. The OD inside and outside the bag was monitored after 30 h to assess the growth of both populations. **d**, Outside the dialysis bag, after 30 h, the OD of the original planktonic fraction (blue cells in **b**) did not increase, while inside the bag, the planktonic OD (teal cells) increased ~3-fold, correspondingly to our expectation for a 30-h period with a population increase rate of $\lambda \approx 0.06$ h^{-1}.

Fig. 4), cells rapidly attached to or detached from the particle surfaces (Supplementary Video 1), suggesting a dynamic equilibration between the subpopulations of planktonic and surface-associated cells[27]. The detachment dynamics were directly quantified by re-incubating pre-colonized particles in fresh media and observing the subsequent accumulation of planktonic cells. We found a rapid detachment rate with $k_d \approx 0.18$ h^{-1} (Extended Data Fig. 5b).

The rate of the reverse process, that is, the attachment of planktonic cells to chitin particles, is difficult to measure directly due to the difficulty of quantifying a low number of cells on particles. Instead, we estimated this rate using a population model describing the dynamics of two subpopulations of densities ρ_b and ρ_s, exchanging with attachment and detachment rates, k_a and k_d, respectively. Importantly, only particle-associated cells replicate (Fig. 2a), with a rate r_s as shown in the following equations:

$$\frac{d\rho_b}{dt} = k_d\rho_s - k_a\rho_b \tag{1}$$

$$\frac{d\rho_s}{dt} = (r_s - k_d)\rho_s + k_a\rho_b. \tag{2}$$

This model admits a dynamic steady state where both subpopulations increase exponentially at the same rate λ, with the fraction of the planktonic subpopulation given by $\rho_b{:}\rho_{\text{total}} = k_d/(\lambda + k_a + k_d)$. Given our measurements of k_d and λ above, the planktonic fraction has an upper bound set by $k_a \to 0$, that is, $\rho_b{:}\rho_{\text{total}} \leq k_d/(\lambda + k_d) \approx 0.7 \pm 0.1$. Comparison to direct measurements of the planktonic fraction $\rho_b{:}\rho_{\text{total}} \approx 0.75{-}0.8$ (Fig. 1d and Extended Data Fig. 1d) suggests that the system is close to this upper bound and thus k_a is negligible.

We validated this via an independent experiment, which established a more stringent bound. By continuously removing the planktonic fraction (shed from the particles) from the chitin culture, we effectively experimentally set $k_a \approx 0$ (Extended Data Fig. 5c). We found that the population growth rate obtained in this experiment corresponded to the one measured in the full chitin culture (Extended Data Fig. 5d,e), corroborating the slowness of attachment with a more stringent bound $k_a \ll \lambda \rho_s/\rho_b$.

Secreted chitinases are enriched on chitin particles

With attachment kinetics being negligible, the steady state in the chitin culture (Fig. 1c) resulting in exponential growth is obtained by the balance between the replication rate of particle-associated cells, r_s, and their detachment rate, k_d, with:

$$\lambda = r_s - k_d. \qquad (3)$$

This is the simple statement that cells on particles must replicate fast enough to sustain their rapid detachment rate. Our measured values for λ (Fig. 1b,c) and k_d (Extended Data Fig. 5b) lead to the estimate $r_s \approx 0.24 \pm 0.04$ h^{-1}, which although much faster than λ, is only one third of the observed maximum growth rate on GlcNAc monomers, $r_{\max} \approx 0.8$ h^{-1} (Fig. 1b). Thus, the slow rate of population increase (compared with $r_{\max}$) in our chitin culture resulted from a high detachment rate k_d on top of a moderate replication rate r_s.

To understand the source of the reduction of the replication rate from $r_{\max}$, we turn our attention to the generation of labile substrates such as GlcNAc monomers and oligomers, since their concentrations determine how fast cells replicate. 1A01's genome is annotated with three chitinases[31]. As different marine bacteria either secrete[16,17,32,33] their chitinases extra-cellularly or keep them bound to their cell surface[15,16,32,34], we first established that 1A01 secreted its chitinases extra-cellularly (Extended Data Fig. 6a) and that these chitinases were strongly associated with chitin particles (Extended Data Fig. 6b). We next characterized the stability of the secreted chitinases by isolating them from the cultures' supernatant (see Fractionation in Methods) and incubating them with fresh chitin particles. There was no significant difference between the chitinolytic activity measured immediately after the enzymes were collected and the activity 24 h later (Extended Data Fig. 6c), thus ruling out significant protein degradation.

A simple relation connects growth to chitinase synthesis

To gain a mechanistic understanding of processes fuelling the replication of particle-associated cells, we follow the flow of labile nutrients (collectively referred to as GlcNAc) in the culture. This nutrient flux generated by the secreted chitinases on the particles, J_n, is taken up by surface-associated cells for their own replication with a flux J_{rep}, as well as for the synthesis of chitinases with a flux J_E (Fig. 3a). In this picture, $J_n = \kappa_E m_E \varepsilon_s$ with ε_s denoting the concentration of chitinases, κ_E the catalytic rate per enzyme mass and m_E the enzyme mass. In our steady-state culture, the nutrient generation flux as well as the biomass (both cellular and extracellular) increase exponentially, outpacing any loss that may be due to diffusion, j_{loss}, or transient mismatches in the two fluxes due to heterogeneity in spatial localization of cells and chitinases (Supplementary Note III). This is consistent with the observed lack of GlcNAc in the medium as well as the lack of replication by planktonic cells (Fig. 2), leading to $J_n = J_{\text{rep}} + J_E$.
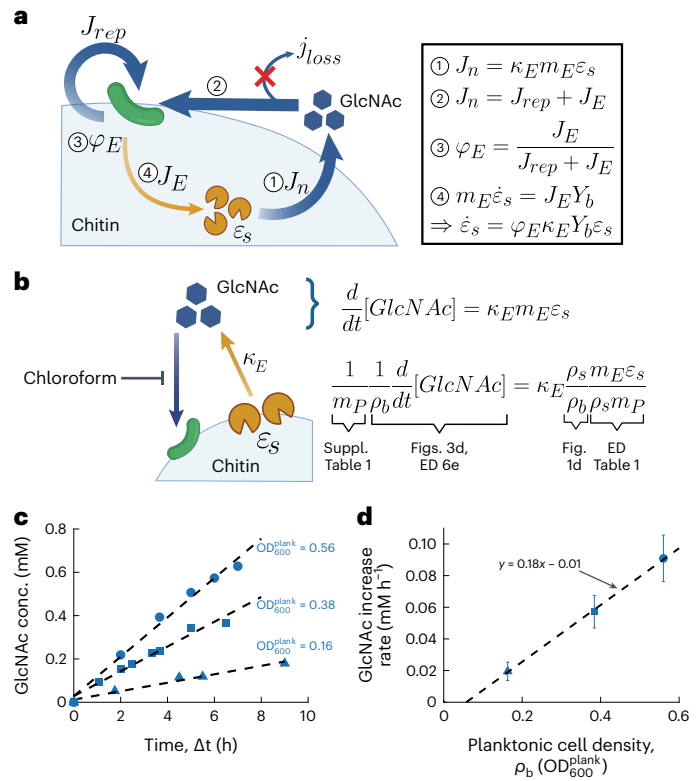
Fig. 3 | Chitinase activity and the resulting carbon flow. a, Model describing chitinase synthesis and labile nutrient generation by chitinases. ① Enzymes attached to the surface of the particles, of concentration ε_s (yellow pacmans), produce GlcNAc molecules (blue hexagons) at a flux $m_E \kappa_E \varepsilon_s$, where κ_E is the catalytic rate of the chitinases per enzyme mass and m_E the enzyme mass. ② The total flux of generated nutrients J_n is partitioned between cellular biomass production J_{rep} and enzyme production J_E since the loss of nutrients due to diffusion j_{loss} is negligible during the exponential phase (see text). ③ The fraction of the total flux J_n allocated towards chitinase synthesis is φ_E; this is a key control parameter set by the cells. ④ The rate of enzyme production $m_E \dot{\varepsilon}_s$ is given by the flux dedicated to enzyme synthesis J_E, with a nutrient-to-biomass conversion factor Y_b. Taken together, relations ① through ④ lead to the equation describing the rate of chitinase synthesis $\dot{\varepsilon}_s = \varphi_E \kappa_E Y_b \varepsilon_s$, which results in the central equation of our study, equation (6), for an exponentially increasing culture limited by labile nutrient generation from chitin. **b**, A simple model of enzyme kinetics. Using a low amount of chloroform (see enzymatic activity in Methods and Extended Data Fig. 6d), we disabled the cells' ability to absorb labile nutrients. This enabled us to measure the activity of the enzymes (yellow pacmans) by tracking the accumulation of GlcNAc (blue hexagons) concentration in the medium at various time intervals. The specific catalytic rate κ_E can be determined from the rate of accumulation of GlcNAc in the medium (**c**,**d**) and the measured chitinase abundance (Extended Data Table 1) through the equations displayed. **c**, GlcNAc concentration is seen to accumulate linearly in time with a rate that varies with the planktonic OD at sampling, reflecting the different amounts of chitinases. The dashed lines represent linear fits to the data, with the flux of GlcNAc generation obtained as the slope of these fits. We note that no GlcNAc oligomers were detected using our procedure, hence we focus on GlcNAc as the primary labile nutrient in this study. We note that the concentrations measured cannot be spatially resolved and are an average for the entire culture. **d**, Flux of GlcNAc generation for samples taken at various planktonic OD shown in **c**. The data points represent the slope of the line of best fit performed in **c** and the error bars represent the 95% confidence intervals of these fits. Fits were performed on sample sizes of at least $n = 5$. The flux increases linearly with the planktonic OD at sampling. The slope of the linear fit adjusted to the -3.3-fold inhibitory effect of chloroform on chitinases (Extended Data Fig. 6d) gives the estimate of $\rho_b^{-1} \frac{d}{dt}[GlcNAc] \approx 0.6$ mM h^{-1} per OD$_{600}^{\text{plank}}$.

Together with the abundance of chitinases on particles, $m_E \varepsilon_s/(\rho_s m_P) \approx 20\%$ and $m_P \approx 300$ μg ml^{-1} per OD600 (Extended Data Table 1), we find $\kappa_E \approx 24 \pm 5$ nmol GlcNAc μg chitinase^{-1} h^{-1}.
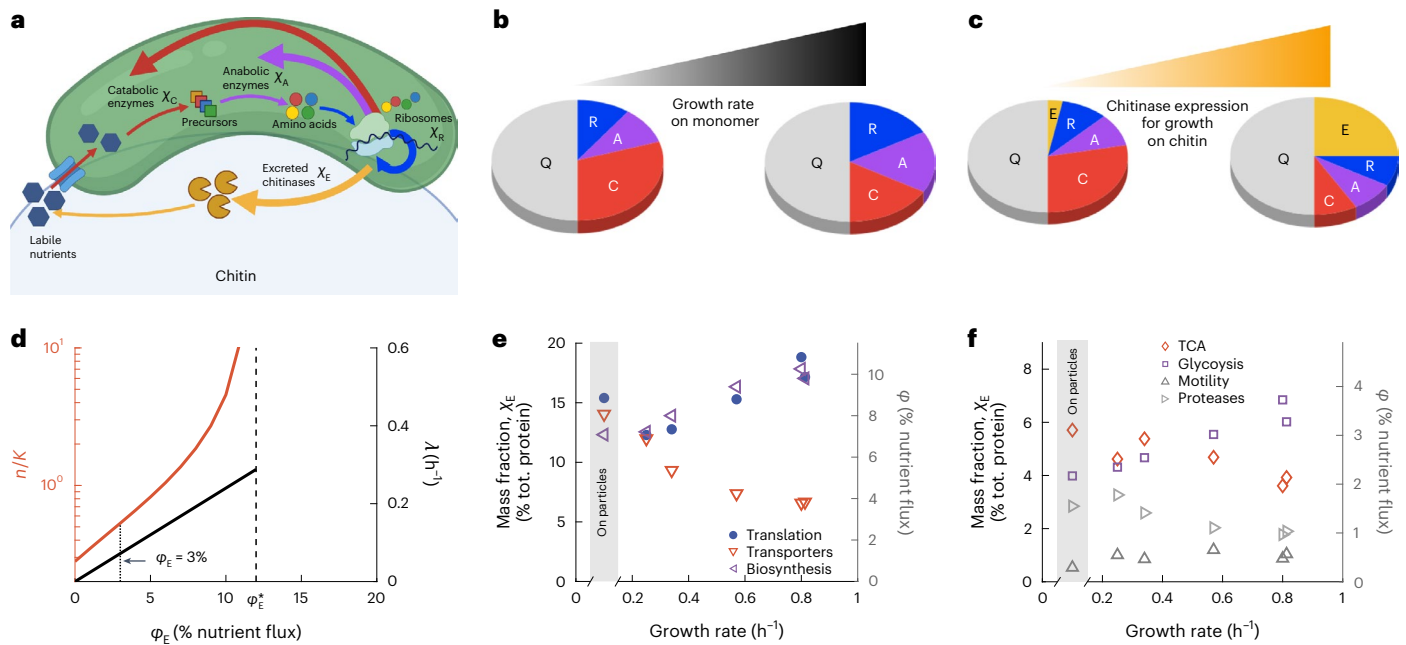
Fig. 4 | Chitinase expression and proteome allocation. a, Illustration of nutrient flow (thin arrows) and protein allocation (thick arrows). Nutrients are generated by **E**xcreted chitinases, taken up and broken down into precursors by **C**atabolic proteins. They are turned into amino acids and nucleotides by **A**nabolic enzymes. Amino acids are assembled by **R**ibosomes and other components of the translational apparatus (R-proteins). C-, A- and R-proteins are synthesized with fractions χ_C, χ_A and χ_R of the total protein synthesis flux, respectively, while chitinases (E-sector) are synthesized with a fraction χ_E. The protein synthesis fraction χ_i is related to the nutrient allocation flux φ_i (discussed in the text) through the protein:biomass ratio, $b = m_p/m_{cell}$ (Supplementary Table 1), by the relation $\varphi_i = b\chi_i/(1-(1-b)\chi_i)$; see Supplementary Note I-1. **b**, Proteome change for growth on good (fast growth) and poor (slow growth) carbon sources based on previous studies of *E. coli*[38,39]. Each wedge of the pie-chart indicates the size of the corresponding fraction χ introduced in **a**. On poor carbon sources, protein synthesis is allocated preferentially towards C-proteins (red), reducing the allocation to R- (blue) and A- (purple) proteins. **c**, Even though the synthesis of chitinases (gold wedge) increases the production of nutrients,

it reduces the allocation towards the C-, A- and R-proteins, which adversely affects growth as described by equation (7). **d**, Solution to equations (5–7) for various levels of chitinase expression, φ_E. The black line indicates the overall population increase rate λ (right axis) and the orange line indicates the nutrient concentration on the surface of chitin (left axis). The nutrient concentration diverges for $\varphi_E = \varphi_E^* \approx 15\%$ (dashed line). The dotted line represents the measured chitinase fraction of $\varphi_E \approx 3\%$ (see Extended Data Table 1), which is well below φ_E^*. The corresponding nutrient concentration is $n/K \approx 0.4$. **e**,**f**, Abundances of proteins belonging to various functional groups (as obtained from mass spectrometry) plotted against the growth rate on various carbon sources (Extended Data Fig. 1a and Supplementary Table 2). We note that the translational group reflects the behaviour of the R-sector, the functional groups for biosynthesis and glycolysis reflect the A-sector, while transporters, TCA and motility reflect the C-sector, analogous to what was found for *E. coli*[38,39]. Data in the grey box correspond to samples associated with particles, with chitinases excluded since they are secreted.

It is convenient to introduce the quantity

$$\varphi_E \equiv \frac{J_E}{J_{rep} + J_E}, \tag{5}$$

which describes the fraction of the total nutrient flux taken up ($J_{rep} + J_E$) that is allocated to chitinase synthesis. Since J_E is the flux of nutrients directed towards chitinase synthesis, we have $m_E\dot{\varepsilon}_s = J_E Y_b$, where Y_b is the biomass yield (Supplementary Table 1). Rewriting equation (5) as $J_E = \varphi_E J_n = \varphi_E \kappa_E m_E \varepsilon_s$, we obtain $\dot{\varepsilon}_s = \varphi_E \kappa_E \varepsilon_s Y_b$, with the steady-state solution:

$$\lambda(\varphi_E) = \varphi_E \kappa_E Y_b. \tag{6}$$

The simple linear relation equation (6) makes explicit a key metabolic constraint governing chitin-dependent growth: if the nutrient generated by the chitinases is growth-limiting, then the growth rate of the system is controlled by the allocation towards chitinase synthesis (see Supplementary Note I-2). This is analogous to the well-known bacterial growth law describing a linear relation between ribosome content and growth rate, where allocation for ribosome biogenesis is the growth-limiting constraint[35–37].

To test the validity of equation (6), we separately quantified φ_E and κ_E to check whether the expression levels and enzymatic properties of

the chitinases account for the observed population increase rate. The flux fraction φ_E can be obtained using mass spectrometry. From the mass fraction of chitinases among the total biomass on the particles (~20%, Extended Data Table 1), we obtain $\varphi_E \approx 3\%$ (see footnote c, Supplementary Table 1).

We next determined the in situ catalytic rate of the chitinases, κ_E. By inhibiting GlcNAc uptake by the cells (Fig. 3b), we tracked the accumulation of GlcNAc in the medium at different planktonic ODs (Fig. 3c). The GlcNAc synthesis rate obtained (Fig. 3d), together with the aforementioned abundance of chitinases on particles, led us to a specific chitinolytic rate, $\kappa_E \approx 24 \pm 5$ nmol GlcNAc µg^{-1} chitinase h^{-1} (Supplementary Table 1). Putting these results together, we find the product $\varphi_E \kappa_E Y_b$ to be 0.07 ± 0.01 h^{-1}, which is comparable to the directly measured growth rate, $\lambda = 0.06 \pm 0.01$ h^{-1}, thus quantitatively supporting equation (6).

Cost and benefit of chitinase expression

Given the maximal replication rate of $r_{max} \approx 0.8$ h^{-1} on GlcNAc monomers (Fig. 1b) and the measured detachment rate of $k_d \approx 0.2$ h^{-1} (Extended Data Fig. 5b), the theoretical maximum growth rate of the chitin culture is $\lambda_{max} = r_{max} - k_d \approx 0.6$ h^{-1} according to equation (3). We next examine why the observed growth rate λ is 10 times below its upper bound λ_{max}.

According to equation (6), the slowness of the growth rate λ may arise from either a slow catalytic rate κ_E or a small allocation

towards chitinase synthesis, φ_E. The catalytic rate κ_E obtained, which works out to be ~0.8 GlcNAc molecules per enzyme per second, is actually well within the activity range measured for other metabolic enzymes[23]. This suggests that chitinase expression (φ_E) may be the primary growth-limiting factor.

But how large can the allocation towards chitinase synthesis be? While chitinases are essential for generating labile nutrients (GlcNAc) equation (6), their biosynthesis constitutes a burden for processes downstream of GlcNAc generation, including GlcNAc uptake, catabolism and other biosynthetic processes (Fig. 4a–c). This view[36] leads us to model these two competing effects of chitinase synthesis on the replication rate r_s of particle-associated cells as:

$$r_s(n, \varphi_E) = r_{max} \frac{n}{n + K} \cdot \left(1 - \frac{\varphi_E}{\varphi_{max}}\right). \qquad (7)$$

Here n is the GlcNAc concentration, r_{max} is the aforementioned saturated growth rate on GlcNAc, K the Monod constant and $\varphi_{max} \approx 30–40\%$ of the maximum fraction of nutrient influx (footnote e, Supplementary Table 1) dedicated to replication in the fastest growth condition (Supplementary Note I).

Equations (3), (6) and (7) can be used to solve for the growth rate λ for arbitrary values of the allocation φ_E. The result (black line in Fig. 4d) shows a positive dependence between the two quantities despite the cost factor in equation (7). This is because the benefit of increasing φ_E as shown by an increasing nutrient concentration n (red line in Fig. 4d) strongly compensates for the cost of chitinase synthesis, until φ_E reaches a maximum of $\varphi_E^* \approx 13\%$ (dashed line in Fig. 4d) when the GlcNAc concentration, n, diverges. This corresponds to the replication rate reaching its maximal value: $r_s^* = r_{max} \cdot (1 - \varphi_E^*/\varphi_{max}) \approx 0.44$ h^{-1} with $\lambda^* = r_s^* - k_d \approx 0.26$ h^{-1}. If φ_E is increased beyond φ_E^*, then the replication rate and hence λ would decrease according to equation (7) since n remains divergent. Thus, φ_E^* is the 'optimal' level of chitinase expression where the growth rate is at its maximum, λ^*.

Culture growth is nutrient-limited due to low chitinase levels

The proteomic trade-off between chitinases and growth enzymes would result in the reduction of the culture's maximum growth rate from $\lambda_{max} \approx 0.6$ h^{-1} to $\lambda^* \approx 0.26$ h^{-1}. Nonetheless, λ^* is still 3.5 times larger than the observed growth rate $\lambda \approx 0.06$ h^{-1} (Fig. 1b,c). Given that the observed chitinase allocation fraction $\varphi_E \approx 3\%$ is well below the 'optimal' allocation $\varphi_E^* \approx 13\%$, we attribute the reduction in growth rate to a low nutrient concentration as per equation (7). For the measured $\varphi_E = 3\%$, our model predicts a nutrient concentration of $n/K \approx 0.4$, suggesting that the slow growth is a consequence of low nutrient concentration, which itself results from a low chitinase expression.

The predicted range of n/K puts the GlcNAc concentration on the surface of the particles in the μM range, given the estimated value of K (Fig. 4d). Because nutrient limitation is directly reflected in the proteome composition of exponentially growing cells[38,39] (Fig. 4b,c), we compared the composition of the proteome of surface-associated cells (excluding chitinases) to that of cells grown under carbon sources that span a range of growth rates from 0.25 h^{-1} to 0.8 h^{-1}. We found that a number of proteins whose abundances increased many folds in slow growth had similarly high abundances on particles (Extended Data Fig. 7a). This is also the case for several major groups of metabolic enzymes showing strong growth-rate dependences, with abundances on the particles more closely resembling those on poor carbon sources (open symbols in Fig. 4e,f). Similar conclusions could be drawn from a more global approach, where the overall proteome of surface-associated cells was more correlated with growth on poor carbon sources (Extended Data Fig. 7c,e). Together, these elements corroborate the finding that the replication rate of particle-associated cells was carbon-limited.
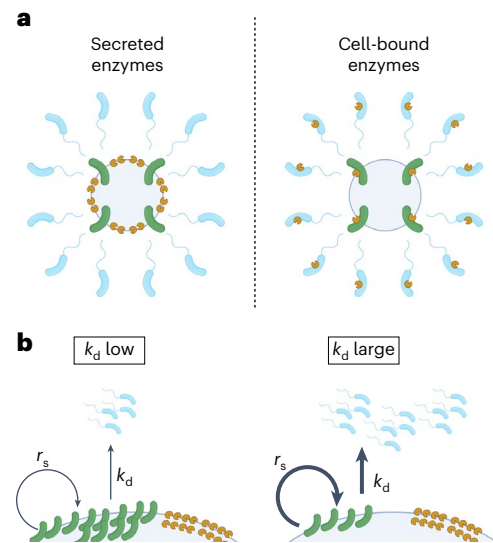

Fig. 5 | Enzyme secretion is coupled to high dispersal. a, Contrasting the cases of secreted and cell-bound enzymes. Secreting enzymes ensures their continued usefulness since they remain attached to the particles even after cells have departed, increasing the chitinase-to-cell ratio on the surface of particles. On the other hand, cell-bound enzymes become 'useless' as soon as cells depart from the particles, resulting in a misallocation of the proteome with a fixed chitinase-to-cell ratio. The difference between these two strategies is modelled in Supplementary Note II and Fig. N-II therein. **b,** Enzyme inheritance illustrates the benefits of chitinase secretion. A higher detachment rate results in fewer cells on the surface of the particles, thus increasing the replication rate r_s through the chitinase-to-cell ratio ε_s/ρ_s. We can see this more formally. In the case of secreted enzymes, $\chi_E = \varepsilon_s/\rho_{total}$. Since the replication rate is proportional to the chitinase amount per cell, this leads to $r_s \propto \chi_E/(\rho_s;\rho_{total})$ where $\rho_s;\rho_{total} = \lambda/(\lambda + k_d)$ is the fraction of the total population remaining on the particles. For higher detachment rates, k_d, this fraction decreases, resulting in more chitinases per cell, which translates to a higher replication rate of these cells. This simple feedback between the detachment rate and the replication rate allows for the chitinase expression per cell to be reduced (since the chitinase production is shared by the entire population).

Discussion

In this study, we characterized the properties of *Vibrio* sp. 1A01 utilizing chitin particles. Despite the heterogeneous nature of the substrate, the culture exhibited simple exponential growth. Quantitative experiments established that in this steady state, the culture segregated into two subpopulations in dynamic equilibrium with each other. Particle-associated cells, although constituting only 1/4 of the population, fuelled the increase of the entire culture by secreting chitinases, replicating and eventually shedding from particles, thereby converting to the planktonic subpopulation which did not replicate nor synthesize chitinases. The overall rate of increase of the culture ($\lambda \approx 0.06$ h^{-1}) was about 1/3 of the rate of detachment of cells from particles ($k_d \approx 0.2$ h^{-1}), with a much smaller rate of attachment. In addition, the replication rate of surface-associated cells, $r_s = \lambda + k_d \approx 0.26$ h^{-1}, was slow relative to their replication on a saturating amount of GlcNAc ($r_{max} \approx 0.8$ h^{-1}). These results are surprising with respect to the canonical scenario for chitin degradation: instead of attaching and consuming the particles until these are nearly exhausted, 1A01 preferentially detached from them, even though they are the sole source of nutrients in the culture. We expect this preferential detachment of 1A01 to hold in the ocean as well, where the particle density is much lower[14], making attachment even less favoured.

Remarkably, the small fraction of particle-associated cells was able to drive the exponential increase of the entire population. We analysed this phenomenon in light of a mechanistic model of chitin utilization,

which led to a central relation (equation (6)) linking chitinase abundance and activity to growth rate. Given the specific chitinase activity measured (κ_ε ~ 1 GlcNAc per enzyme per second which was not particularly low[23]), we expect that increasing chitinase production would result in an increase in growth rate until an upper bound $\lambda^* = 0.26$ h^{-1} (Fig. 4d). We attribute the slow growth observed, $\lambda \approx \lambda^*/4$, to the low level of chitinase excretion, estimated to be $\varphi_E \approx 3\%$ of the total nutrient flux. This low level of chitinase production could be due to a proteomic cost not probed in this analysis (for example, secretion machinery), or a strategy to mitigate 'cheating' (see below) since higher chitinase expression would result in higher nutrient concentration (Fig. 4d), making it more accessible to other species. Alternatively, slow growth may be favoured for ecological reasons in the context of sinking particulate organic matter (POM) (see Extended Data Fig. 8).

The extracellular secretion and release of precious, growth-limiting resources is commonly thought of as wasteful from the perspective of the secreting individual as it results in the production of public goods that may escape capture and promote 'cheating'. As a way of bypassing this problem, organisms may 'privatize' their resources by binding them to the cell surface[16,40–42] such that nutrients generated are immediately taken up. Our analysis in Supplementary Note I-2 suggests that such a strategy would be inefficient from a resource allocation perspective as it would require chitinase expression to increase 4-fold to $\varphi_E \approx 12\%$ to support the same growth rate, λ (Supplementary Note I-4). This inefficiency arises because cells with bound enzymes would carry their enzymes with them as they detach from particles, after which these enzymes become 'useless' (Fig. 5a). This highlights a fundamental conflict between 'privatizing' enzymes to prevent 'cheating' and secreting enzymes to enable rapid dispersal while maintaining growth.

Conversely, the coupling between enzyme secretion and rapid dispersal is advantageous (Fig. 5b). This is because for the same level of chitinase expression, an increase in cell detachment leads to fewer cells on particles, thus higher enzyme-to-cell ratio and higher flux of nutrient generation and higher rate of cell replication on particles. This non-intuitive effect, that increasing dispersal leads to higher on-particle replication rate, is a result of cells on particles 'inheriting' enzymes synthesized by their departing relatives. This mechanism underlies the key relation, equation (6), which dictates that the population increase rate is independent of the cell detachment rate (up to the maximal possible rate λ^*). This enzyme inheritance mechanism ensures that the remaining on-particle colonies maintain high replication rates despite large amount of dispersal. By decoupling cellular replication from nutrient production through the extracellular release of enzymes, the population as a whole can circumvent the colonization–dispersal trade-off that individual cells are subjected to.

Through quantitative characterization of bacterial growth and protein allocation on and away from particles for *Vibrio* sp. 1A01, this study has revealed a simple molecular trick—the release and inheritance of chitinases—which decouples the commonly held trade-off between growth and dispersal at the population level. These two population traits can instead be independently set by various environmental factors (Extended Data Fig. 9), illustrating the intricate interplay between bacterial strategies of substrate utilization and population dynamics in spatially structured nutrient landscapes.

Methods

Strain

Vibrio sp. 1A01 was previously isolated[30] from an enrichment of coastal seawater (Nahant, Massachusetts) on chitin beads and obtained from the Cordero lab. It was maintained in glycerol stocks. Colonies were streaked on Marine Broth 2216 with 1.5% agar plates.

Growth experiments

Experiments were carried out in three steps: seed culture in Marine Broth 2216, pre-culture and experimental culture in the identical minimal medium. For the seed culture, single colonies were inoculated into liquid Marine Broth 2216 media until they reached a sizeable density and then transferred to the pre-culture media with either chitin flakes or the designated substrate as a carbon source. Cells were incubated in the pre-culture medium for about 10 doublings (4 d for chitin cultures) and then transferred to the experimental culture for all assays. For chitin cultures, particles were sedimented (see methods below) and the planktonic fraction only was used to begin a new experimental culture.

Culture conditions

Cells were grown in a minimal seawater medium. The base medium used was from ref. 43. To reproduce the osmolarity of seawater, it contained 340 mM NaCl, 15 mM MgCl$_2$, 6.75 mM KCl and 1 mM CaCl$_2$. To reproduce the pH in the ocean, it was buffered using 40 mM HEPES salt at pH 8.2. The nitrogen source was 10 mM ammonium chloride, the phosphorous source 100 mM sodium phosphate and the sulfur source 1 mM sodium sulfate. In addition, the medium was supplemented with a mix of trace metals (see ref. 43 for full list). Most importantly it contained 1 mg l^{-1} of iron, which was chelated with 4 mM tricine. This medium was supplemented with 0.2% w/v chitin flakes (Sigma C9213) or the corresponding carbon source as indicated. Depending on the culture volume, 50 ml conical tubes (VWR, 89038-658) (for 10 ml cultures) or 500 ml glass flasks (for 100 ml cultures) were used to minimize chitin particles sticking to the walls. Cultures were incubated in water bath shakers at 27 °C and shaken at 250 r.p.m.

Fractionation of the culture

Many of our experiments relied on separating the components of the culture as shown in Fig. 1. These components are planktonic cells, particles which contain both cells and excreted proteins, and the supernatant which contains excreted proteins.

Particle–plankton separation. To separate particles from the planktonic phase, samples were taken from the culture with large-bore tips (Thermo Scientific, 21-236-1A) and spun at a low speed of ~25 g for a short amount of time to sediment the particles. The planktonic phase was carefully pipetted out and separated from the remaining particles for further processing.

Supernatant extraction. To isolate the supernatant, samples of our culture were passed through a 0.22-μm-pore vacuum filter (SteriCup Quick Release 150 ml S2GPU02RE). To concentrate the excreted proteins, aliquoted samples of the supernatant were spun in 3 kDa concentrators (Amicon-Ultra C7715) in a refrigerated tabletop centrifuge at ~2,270 g for 1 h, consolidated and spun again until ~100× concentration in volume was achieved. The extracted and concentrated samples were kept at 4 °C until use, but not longer than a day.

Planktonic OD

Samples (500 μl) were taken from the cultures using P1000 pipette tips to make sure chitin particles did not clog the tips and transferred to 2 ml Eppendorf tubes. Tubes were centrifuged at 25 g on a tabletop centrifuge to sediment the chitin particles. Of the planktonic phase, 200 μl were used to determine the planktonic OD of the culture at 600 nm using a Genesys 30 spectrophotometer.

Microscopy

Samples (200 μl) were taken from exponentially growing chitin cultures and fractionated into particles or planktonic cells if needed. Chitin flakes were stained with 1 μg ml^{-1} FITC-WGA and cells were stained with a membrane dye FM 4-64 with a concentration of 5 μg ml^{-1}. The culture was then fixed with phosphate buffered glutaraldehyde and transferred to a chitin chamber for imaging. The chitin chamber was assembled by appending a precut double-sided 3M tape to a cover

glass and then sealed with a cover slip. Chambers were imaged using a Leica TCS SP8 inverted confocal microscope. The WGA signal was read in the GFP channel, which was excited with a 488 nm diode laser and the FM 4-64 was read in the mCherry channel and excited with a 580 nm diode laser. Fluorescence for both channels was detected through a ×40/1.3 objective and a highly sensitive HyD SP GaAsP detector.

Dialysis bag experiment

The planktonic and particle components of an exponentially growing chitin culture were separated as described above. In brief, 10 ml of culture was separated from the particles, which were then resuspended in 10 ml of chitin-free media. The OD of the resuspended particles was measured and the particles transferred to a 14 kDa MWCO dialysis tube (Sigma D0405) secured with clips. The tube was then inserted in a 500 ml glass flask filled with the planktonic component. The flask was incubated in a water bath at 27 °C with shaking at 250 r.p.m. The OD outside the dialysis bag was determined periodically. However, the planktonic OD inside the bag could only be determined at the end of the experiment upon the reopening of the clips securing the tubing.

Detachment rate

From exponentially growing chitin cultures from which we noted the planktonic OD, the planktonic component was separated from the particles using the method described above. Collected particles were then resuspended in the same volume of fresh, chitin-free media. The planktonic OD of this resulting culture was monitored at regular time intervals. The detachment rate was obtained from the slope of the linear fit of the resulting data.

^{32}P incorporation[44]

^{32}P-orthophosphate (Perkin Elmer) was added to exponentially growing chitin cultures at 3 μCi ml^{-1} and labelling was carried for 2–3 generations before collecting samples. Samples of the total culture or of only the planktonic fraction (200 μl) were pelleted, washed once with the media buffer and frozen. They were subsequently thawed and resuspended in 2 ml of scintillation cocktail (Liquiscint, National Diagnostics). Radiolabel incorporation was estimated as counts per minute using a Beckmann LS6500 scintillation counter.

Protein measurements

The method for the biuret assay was adapted from ref. 45. From an exponentially growing culture of either the full samples, planktonic samples only or particles only, 1.5 ml was pelleted, washed, resuspended in 200 μl of carbonless media buffer, fast frozen on dry ice and stored. For measurements of extracellular protein amounts, 200 μl of the concentrated supernatant (see method above) was used. Samples were thawed and the protein concentration measured using the biuret assay. In brief, 0.1 ml of 3 M NaOH was added to the cell pellet and samples were incubated at 100 °C on a heat block for 5 min to lyse the cells and hydrolyse the proteins. Samples were then cooled at room temperature for 5 min. The biuret reactions were carried out by adding 0.1 ml 1.6% CuSO$_4$ to the samples with thorough mixing at r.t. for 5 min. Samples were then centrifuged and the absorbance at 555 nm was measured using a spectrophotometer. The same reaction was applied to a series of BSA standards of concentrations ranging from 0–5 mg ml^{-1} and a standard curve established. Protein amounts in the experimental samples were determined using this standard curve.

RNA measurement

The method of RNA measurement was adapted from refs. 46,47 with modifications. For the chitin condition, these experiments were performed in 100 ml culture volume with shaking in 500 ml glass flasks. From an exponentially growing culture of either the full samples, planktonic samples only or particles only, 1.5 ml was pelleted, fast frozen on dry ice and stored. Pellets were thawed and washed twice with 0.7 M cold HClO$_4$, then digested for 60 min at 37 °C using 300 μl 0.3 M KOH. Samples were periodically stirred. The cell extracts were then neutralized with 100 μl 3 M HClO$_4$ and centrifuged at 13,000 r.p.m. (16,300g) for 3 min. The soluble fraction was collected and the remaining pellets washed twice with 550 μl 0.5 M HClO$_4$. The resulting final volume of 1.5 ml was centrifuged once more to eliminate remaining debris and its absorbance at 260 nm was measured using a Bio-Rad spectrophotometer. The RNA concentration was determined as $31 OD_{260}/OD_{600}$ where the conversion factor is based on RNA's extinction coefficient.

RNA synthesis rate measurement

RNA synthesis rate measurement was performed as previously described[48], with the following modifications. To measure the RNA synthesis rate of the full culture, 100 μl cultures were dispensed into 6 microfuge tubes from a well-suspended chitin culture. To each tube, 5 μCi of ^{3}H-uridine (Perkin Elmer) was added ($t = 0$) and labelling was allowed to continue in the different tubes for different durations (30 s, 60 s, 90 s, 120 s, 150 s and 180 s). Labelling was stopped by adding 100 μl boiling lysis buffer (0.1 M NaCl, 0.01 M Tris, 0.02 M EDTA, 0.5% SDS). Each sample was boiled for 2 min, chilled on ice for 15 min and then RNA was precipitated using an equal volume of ice-cold 10% trichloroacetic acid (TCA).

To measure RNA synthesis rate from planktonic cultures, 1 ml of a well-suspended chitin culture was spun down at low speed (500 r.p.m., 30 s) and 975 μl of the planktonic culture was moved to a fresh microfuge tube containing 5 uCi of ^{3}H-uridine (the moment of addition denoted as $t = 0$). At various time intervals (1 min, 2 min, 3 min, 4 min, 5 min and 6 min), 100 μl samples were moved to boiling lysis buffer and the samples were boiled, chilled and precipitated as described above for the particles. All precipitated samples were added to 2 ml of scintillation cocktail (Liquiscint, National Diagnostics) and label incorporation was measured using a Beckmann LS6500 scintillation counter.

Enzymatic activity

To assay the in situ enzymatic activity of the chitinases, 10 ml samples were taken at various points along the steady-state growth curve on chitin. Chloroform (500 μl) was added to permeabilize the cells and prevent their GlcNAc uptake. The tubes were shaken at 250 r.p.m. in a 27 °C water bath shaker.

To assay the enzymatic activity of samples extracted from the supernatant, equal volumes of the extract were incubated with chitin particles suspended in 10 ml of the culture buffer, shaking at 250 r.p.m. in a 27 °C water bath.

To monitor the enzymatic activity in both cases, 200 μl were sampled from the tubes at regular time intervals and filtered through a 0.22 μm nylon filter centrifuge tube (Corning Costar Spin-X centrifuge tubes). The GlcNAc concentration was then measured from the supernatant using HPLC as outlined below.

HPLC

The HPLC method was adapted from ref. 49. In brief, 80 μl of filtered sample was transferred to HPLC sample tubes and analysed using a Shimadzu Prominence HPLC using RID detection. The HPLC setup was as follows: isocratic HPLC was used with 10 mM H$_2$SO$_4$ as mobile phase at 0.4 ml min^{-1} pump speed; samples were kept at room temperature in the autosampler (Shimadzu SIL-10AF); 20 μl of sample was injected; samples were separated using ion exchange chromatography; the column (Phenomenex, Rezex ROAOrganic Acid H+ (8%), LC column 300 × 7.8 mm) was kept in a column oven (Shimadzu STO-20A) at 40 °C; data from the RID detector (Shimadzu RID-20A) were recorded for 40 min. With these settings, the elution time of GlcNAc was between

19.8 and 20.5 min. Data were subsequently analysed with a custom script in MATLAB. In short, peaks of interest were isolated and their baseline adjusted by linearly interpolating the initial and final intensities of the peak. The area under the corrected peaks was then computed. The concentrations corresponding to given areas under peaks were determined by running standards with known concentrations of the compounds of interest.

SDS–PAGE

Samples (planktonic cells, particles and extracellular proteins) were collected from a steady-state chitin culture using the fractionation method outlined above. Cells were lysed and protein reduced by mixing 25 µl of sample to 4.75 µl Laemmelli buffer (Bio-Rad, 161-0737) and 0.25 µl beta-mercaptoethanol (Bio-Rad, 161-0710) and boiling the reaction at 100 °C for 5 min. Samples (30 µl) were loaded in each well of the pre-cast 10% TGx Mini Protean gels (Bio-Rad, 4568033). The ladder used was 1 µl of Bio-Rad's Precision Plus Dual Color 1610374 with bands ranging from 250–10 kDa and two bands that fluoresce in UV light at 75 and 25 kDa. Running buffer (1 l, Bio-Rad, 161-0732) was added to the cell and the gels were ran for 40 min at 200 V. The stain-free fluorescent gels were activated with UV light for 5 min and then imaged under a UV gel box. Individual bands of interest were excised using a scalpel that was cleaned upon each incision and stored at 4 °C for further processing by mass spectrometry.

Proteomic mass spectrometry

The proteomic mass spectrometry method was adapted from ref. 38. Each sample contained an ^{15}N-labelled reference, which allowed comparison of unlabelled experimental proteins across growth conditions of interest. Each experimental sample in a series was mixed in an equal amount with a known labelled standard sample as reference, and the relative change in protein expression in the experimental sample was obtained for each protein.

Sample collection. For each planktonic culture, 1.5 ml of cell culture at $OD_{600}^{plank} = 0.4 - 0.5$ was collected by centrifugation. For chitin cultures, the particles were separated from the planktonic fraction before pelleting. The cell pellet was resuspended in 0.2 ml of water and fast frozen on dry ice. For the extracellular sample, 200 µl of the 100× concentrate of the supernatant (see extraction method above) was used.

Sample preparation. ^{15}N labelling was achieved by using ^{15}N-labelled ammonia as the sole nitrogen source. A balanced mixture of the two ^{15}N-labelled cell samples (from a glycolytic fast growth condition on glucose and a gluconeogenic slow growth condition on acetate) was prepared as a universal reference. These conditions were chosen to obtain a wide coverage of the proteome without biasing a particular growth condition. Of the reference, 50 µg was mixed with 50 µg of each experimental sample. This balanced preparation (equal amounts of total protein) enabled the measurement of the proteome mass fraction for each protein.

Proteins were precipitated by adding 100% (w/v) TCA to a final concentration of 25%. Samples were left to stand on ice for a minimum of 1 h. The protein precipitates were spun down by centrifugation at 13,200 g for 15 min at 4 °C. The supernatant was removed and the pellets were washed with cold acetone and dried in a Speed-Vac concentrator.

The pellets were dissolved in 80 µl 100 mM NH$_4$HCO$_3$ with 5% acetonitrile. Dithiothreitol (8 µl, 50 mM) was added to reduce the disulfide bonds before the samples were incubated at 65 °C for 10 min. Cysteine residues were modified by adding 8 µl 100 mM iodoacetamide, followed by incubation at 30 °C for 30 min in the dark. Proteolytic digestion was carried out by adding 8 µl 0.1 µg µl^{-1} trypsin (Sigma-Aldrich) with incubation overnight at 37 °C. The peptide solutions were cleaned using PepClean C-18 spin columns (Pierce). After drying in a Speed-Vac concentrator, the peptides were dissolved into 10 µl sample buffer

(5% acetonitrile and 0.1% formic acid). For samples containing chitin particles, only the soluble portion of the pellet was used.

Data acquisition. Data acquisition was adapted from refs. 38,50. MS data were acquired using an AB Sciex 5600 TripleTOF spectrometer with the injection of 2 µg tryptic peptides, with MS1 accumulation time of 250 ms and MS2 accumulation time of 150 ms.

Protein identification. Protein identification was adapted from refs. 38,50. In brief, raw data files (.wiff and .wiff.scan formats) were converted to profile and centroided mzML formats. Centroided mzML files were converted to mzXML using tools included in the Trans-Proteomic Pipeline (TPP) and searched using X!Tandem (Alanine version https://thegpm.org) against the UniProt *Vibrio* sp. 1A01 database (organism ID 314742) supplemented with common protein contaminants, enzymes and reversed peptide decoy sequences. The peptide–spectrum match tolerances were set at 50 ppm and 100 ppm for the precursor and product ions, respectively. The TPP tools PeptideProphet and iProphet were used to score the peptide–spectrum matches and the search results were combined into a consensus library using SpectraST[51].

Relative protein quantification. Relative protein quantitation was adapted from refs. 38,50. Using an in-house quantification software, Massacre (V.P. and J.R.W., unpublished), on the consensus library, we quantified the relative intensities of the ^{14}N (light) peptides to ^{15}N (heavy) peptides. In brief, the intensity for each peptide was integrated over a patch in retention time (RT), m/z space that encloses the envelope for the light and heavy peaks. After collapsing data in the RT dimension, the light and heavy peaks were fit to a multinomial distribution (a function of the chemical formula of each peptide) using a least squares Fourier transform convolution routine, which yields the relative intensity of the light and heavy species. The ratio of the unlabelled to the labelled peak intensity was obtained for each peptide in each sample. A confidence measure for each fit was calculated from a support vector machine trained on a large set of user scoring events.

Absolute protein quantification. The absolute protein level for each sample was obtained by dividing the ^{14}N spectral counts for each protein by the total spectral counts detected in each sample in the ^{14}N channel.

Reporting summary

Further information on research design is available in the Nature Portfolio Reporting Summary linked to this article.

Data availability

The mass spectrometry proteomics data have been deposited to the ProteomeXchange Consortium[52] via the UCSD MassIVE partner repository with the dataset identifier PXD034003. Summary tables including both absolute and relative quantitation as well as functional grouping can be found in Supplementary Tables 2 and 3. All other data that support the findings of this study are available from the corresponding author upon request. Source data are provided with this paper.

References

1. Monod, J. The growth of bacterial cultures. *Annu. Rev. Microbiol.* **3**, 371–394 (1949).
2. Nguyen, T. T. H. et al. Microbes contribute to setting the ocean carbon flux by altering the fate of sinking particulates. *Nat. Commun.* **13**, 1657 (2022).
3. Yawata, Y. et al. Competition–dispersal tradeoff ecologically differentiates recently speciated marine bacterioplankton populations. *Proc. Natl Acad. Sci. USA* **111**, 5622–5627 (2014).
4. Yawata, Y., Carrara, F., Menolascina, F. & Stocker, R. Constrained optimal foraging by marine bacterioplankton on particulate organic matter. *Proc. Natl Acad. Sci. USA* **117**, 25571–25579 (2020).

5. Fernandez, V. I., Yawata, Y. & Stocker, R. A foraging mandala for aquatic microorganisms. *ISME J.* **13**, 563–575 (2019).

6. Pomeroy, L. R. The ocean's food web, a changing paradigm. *BioScience* **24**, 499–504 (1974).

7. Alldredge, A. L. & Gotschalk, C. C. The relative contribution of marine snow of different origins to biological processes in coastal waters. *Cont. Shelf Res.* **10**, 41–58 (1990).

8. Kiørboe, T. & Jackson, G. A. Marine snow, organic solute plumes, and optimal chemosensory behavior of bacteria. *Limnol. Oceanogr.* **46**, 1309–1318 (2001).

9. Gasol, J. M. & Kirchman, D. L. *Microbial Ecology of the Oceans* (John Wiley & Sons, 2018).

10. Azam, F. & Malfatti, F. Microbial structuring of marine ecosystems. *Nat. Rev. Microbiol.* **5**, 782–791 (2007).

11. Souza, C. P., Almeida, B. C., Colwell, R. R. & Rivera, I. N. G. The importance of chitin in the marine environment. *Mar. Biotechnol.* **13**, 823–830 (2011).

12. Grimes, D. J. et al. What genomic sequence information has revealed about *Vibrio* ecology in the ocean—a review. *Microb. Ecol.* **58**, 447–460 (2009).

13. Jollès, P. & Muzzarelli, R. A. A. *Chitin and Chitinases* (Birkhäuser Verlag, 1999).

14. Muzzarelli, R. A. A., Gooday, G. W. & Jeuniaux, C. *Chitin in Nature and Technology* (Plenum Press, 1986).

15. Li, X. & Roseman, S. The chitinolytic cascade in Vibrios is regulated by chitin oligosaccharides and a two-component chitin catabolic sensor/kinase. *Proc. Natl Acad. Sci. USA* **101**, 627–631 (2004).

16. Meibom, K. L. et al. The *Vibrio cholerae* chitin utilization program. *Proc. Natl Acad. Sci. USA* **101**, 2524–2529 (2004).

17. Bassler, B. L., Yu, C., Lee, Y. C. & Roseman, S. Chitin utilization by marine bacteria. Degradation and catabolism of chitin oligosaccharides by *Vibrio furnissii*. *J. Biol. Chem.* **266**, 24276–24286 (1991).

18. Pruzzo, C., Crippa, A., Bertone, S., Pane, L. & Carli, A. Attachment of *Vibrio alginolyticus* to chitin mediated by chitin-binding proteins. *Microbiology* **142**, 2181–2186 (1996).

19. Svitil, A. L., Chadhain, S., Moore, J. A. & Kirchman, D. L. Chitin degradation proteins produced by the marine bacterium *Vibrio harveyi* growing on different forms of chitin. *Appl. Environ. Microbiol.* **63**, 408–413 (1997).

20. Suzuki, K. et al. Chitinases A, B, and C1 of *Serratia marcescens* 2170 produced by recombinant *Escherichia coli*: enzymatic properties and synergism on chitin degradation. *Biosci. Biotechnol. Biochem.* **66**, 1075–1083 (2002).

21. Chuang, H.-H. & Lin, F.-P. New role of C-terminal 30 amino acids on the insoluble chitin hydrolysis in actively engineered chitinase from *Vibrio parahaemolyticus*. *Appl. Microbiol. Biotechnol.* **76**, 123–133 (2007).

22. Svitil, A. L. & Kirchman, D. L. Y. A chitin-binding domain in a marine bacterial chitinase and other microbial chitinases: implications for the ecology and evolution of 1,4-β-glycanases. *Microbiology* **144**, 1299–1308 (1998).

23. Davidi, D. et al. Global characterization of in vivo enzyme catalytic rates and their correspondence to in vitro kcat measurements. *Proc. Natl Acad. Sci. USA* **113**, 3401–3406 (2016).

24. Belas, M. R. & Colwell, R. R. Adsorption kinetics of laterally and polarly flagellated *Vibrio*. *J. Bacteriol.* **151**, 1568–1580 (1982).

25. Nalin, D. R., Daya, V., Reid, A., Levine, M. M. & Cisneros, L. Adsorption and growth of *Vibrio cholerae* on chitin. *Infect. Immun.* **25**, 768–770 (1979).

26. Kaneko, T. & Colwell, R. R. Adsorption of *Vibrio parahaemolyticus* onto chitin and copepods. *Appl. Microbiol.* **29**, 269–274 (1975).

27. Kiørboe, T., Tang, K., Grossart, H.-P. & Ploug, H. Dynamics of microbial communities on marine snow aggregates: colonization, growth, detachment, and grazing mortality of attached bacteria. *Appl. Environ. Microbiol.* **69**, 3036–3047 (2003).

28. Bassler, B., Gibbons, P. & Roseman, S. Chemotaxis to chitin oligosaccharides by *Vibrio furnissii*, a chitinivorous marine bacterium. *Biochem. Biophys. Res. Commun.* **161**, 1172–1176 (1989).

29. Bassler, B. L., Gibbons, P. J., Yu, C. & Roseman, S. Chitin utilization by marine bacteria. Chemotaxis to chitin oligosaccharides by *Vibrio furnissii*. *J. Biol. Chem.* **266**, 24268–24275 (1991).

30. Datta, M. S., Sliwerska, E., Gore, J., Polz, M. F. & Cordero, O. X. Microbial interactions lead to rapid micro-scale successions on model marine particles. *Nat. Commun.* **7**, 11965 (2016).

31. Karp, P. D. et al. The BioCyc collection of microbial genomes and metabolic pathways. *Brief. Bioinform.* **20**, 1085–1093 (2019).

32. Hayes, C. A., Dalia, T. N. & Dalia, A. B. Systematic genetic dissection of chitin degradation and uptake in *Vibrio cholerae*: genetic dissection of chitinases in *V. cholerae*. *Environ. Microbiol.* **19**, 4154–4163 (2017).

33. Leventhal, G. E., Ackermann, M. & Schiessl, K. T. Why microbes secrete molecules to modify their environment: the case of iron-chelating siderophores. *J. R. Soc. Interface* **16**, 20180674 (2019).

34. Aunkham, A. et al. Structural basis for chitin acquisition by marine *Vibrio* species. *Nat. Commun.* **9**, 220 (2018).

35. Maaløe, O. in *Biological Regulation and Development: Gene Expression* (ed. Goldberger, R. F.) 487–542 (Springer, 1979).

36. Scott, M., Gunderson, C. W., Mateescu, E. M., Zhang, Z. & Hwa, T. Interdependence of cell growth and gene expression: origins and consequences. *Science* **330**, 1099–1102 (2010).

37. Neidhardt, F. C. & Magasanik, B. Studies on the role of ribonucleic acid in the growth of bacteria. *Biochim. Biophys. Acta* **42**, 99–116 (1960).

38. Hui, S. et al. Quantitative proteomic analysis reveals a simple strategy of global resource allocation in bacteria. *Mol. Syst. Biol.* **11**, 784 (2015).

39. Mori, M. et al. From coarse to fine: the absolute *Escherichia coli* proteome under diverse growth conditions. *Mol. Syst. Biol.* **17**, e9536 (2021).

40. Itoh, T. et al. Cooperative degradation of chitin by extracellular and cell surface-expressed chitinases from *Paenibacillus* sp. strain FPU-7. *Appl. Environ. Microbiol.* **79**, 7482–7490 (2013).

41. Itoh, T. et al. Overexpression, purification, and characterization of *Paenibacillus* cell surface-expressed chitinase ChiW with two catalytic domains. *Biosci. Biotechnol. Biochem.* **78**, 624–634 (2014).

42. Itoh, T. et al. Crystal structure of chitinase ChiW from *Paenibacillus* sp. str. FPU-7 reveals a novel type of bacterial cell-surface-expressed multi-modular enzyme machinery. *PLoS ONE* **11**, e0167310 (2016).

43. Amarnath, K. et al. Stress-induced metabolic exchanges between complementary bacterial types underly a dynamic mechanism of inter-species stress resistance. *Nat. Commun.* **14**, 3165 (2023).

44. Jansson, M. Phosphate uptake and utilization by bacteria and algae. *Hydrobiologia* **170**, 177–189 (1988).

45. Herbert, D., Phipps, P. J. & Strange, R. E. in *Methods in Microbiology* Vol. 5 (eds Norris, J. R. & Ribbons, D. W.) 209–344 (Academic Press, 1971).

46. You, C. et al. Coordination of bacterial proteome with metabolism by cyclic AMP signalling. *Nature* **500**, 301–306 (2013).

47. Benthin, S., Nielsen, J. & Villadsen, J. A simple and reliable method for the determination of cellular RNA content. *Biotechnol. Tech.* **5**, 39–42 (1991).

48. Balakrishnan, R. et al. Principles of gene regulation quantitatively connect DNA to RNA and proteins in bacteria. *Science* **378**, eabk2066 (2022).

49. Cremer, J., Arnoldini, M. & Hwa, T. Effect of water flow and chemical environment on microbiota growth and composition in the human colon. *Proc. Nat Acad. Sci.* **114**, 6438–6443 (2017).
50. Dai, X. et al. Reduction of translating ribosomes enables *Escherichia coli* to maintain elongation rates during slow growth. *Nat. Microbiol.* **2**, 16231 (2017).
51. Lam, H. et al. Building consensus spectral libraries for peptide identification in proteomics. *Nat. Methods* **5**, 873–875 (2008).
52. Vizcaíno, J. A. et al. ProteomeXchange provides globally coordinated proteomics data submission and dissemination. *Nat. Biotechnol.* **32**, 223–2266 (2014).

Acknowledgements

Author contributions

T.H. and G.G. conceived the study, designed experiments and wrote the manuscript. G.G. conducted all experiments and performed modelling work. R.B. designed, optimized protocols, conducted radioactivity experiments and analysed data. V.P. processed proteomics samples, designed data processing pipelines and analysed data with guidance from J.R.W. T.C. contributed to modelling work. All authors contributed to editing the manuscript.

Competing interests

The authors declare no competing interests.

Additional information

Extended data is available for this paper at https://doi.org/10.1038/s41564-023-01444-5.

Supplementary information The online version contains supplementary material available at https://doi.org/10.1038/s41564-023-01444-5.

Correspondence and requests for materials should be addressed to Terence Hwa.

Peer review information *Nature Microbiology* thanks Alvaro Sanchez, Vaibhhav Sinha, Alma Dal Co and the other, anonymous, reviewer(s) for their contribution to the peer review of this work.

Reprints and permissions information is available at www.nature.com/reprints.

Publisher's note Springer Nature remains neutral with regard to jurisdictional claims in published maps and institutional affiliations.

a

b

$R/\rho = 40r + 50$

c

d
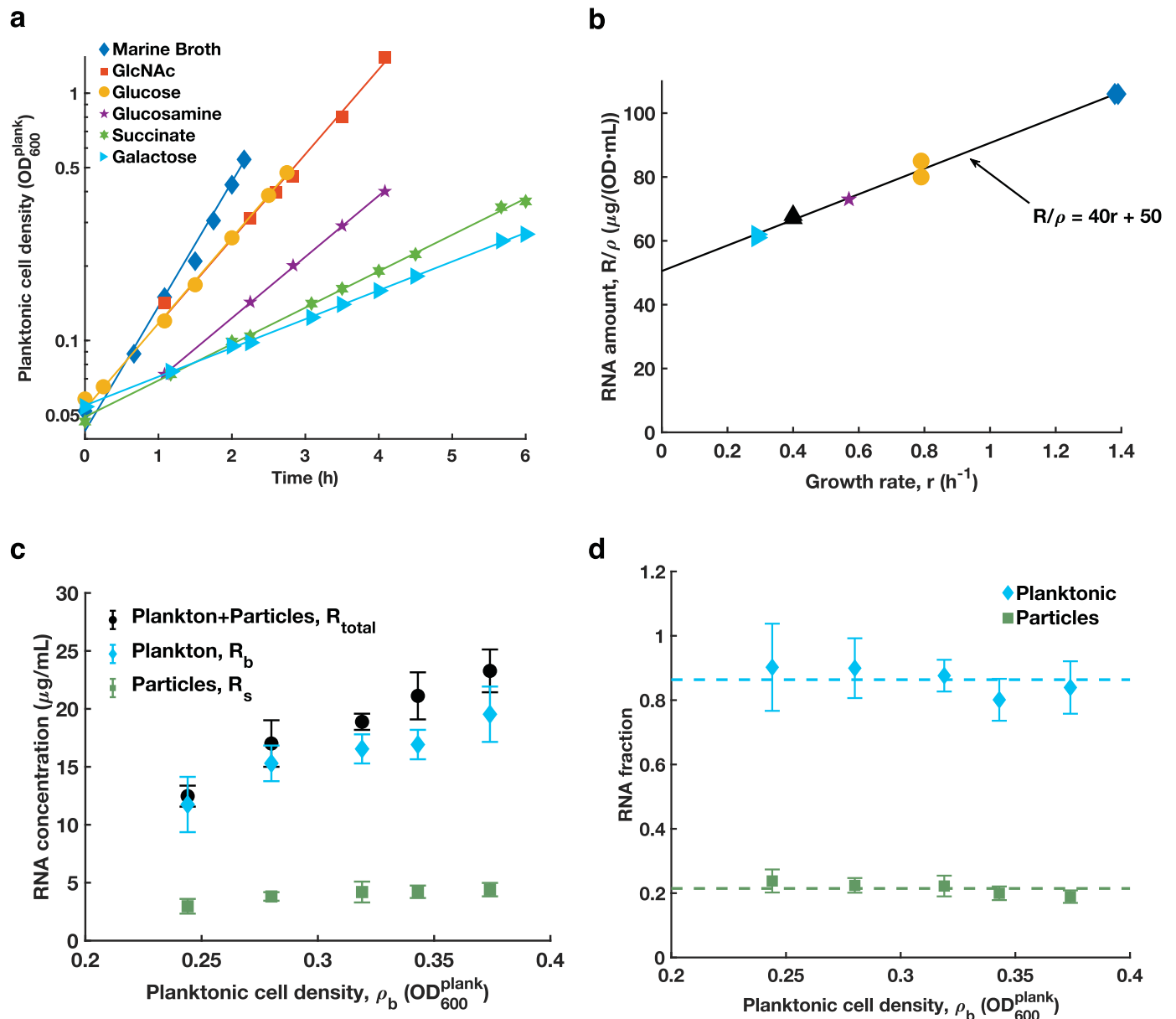
Extended Data Fig. 1 | Quantifying the RNA abundance of cells grown in different conditions. a) Growth curves of 1A01 grown in minimal media with different carbon sources. Cultures were inoculated from exponentially growing pre-cultures with the same carbon source. The replication rates (r) were obtained from the exponential fits and ranged from $1.15\,h^{-1}$ to $0.26\,h^{-1}$; see Supplementary Table 2 for values. **b)** RNA amounts per OD\•mL of culture, R/ρ, was obtained for exponentially growing cultures in different carbon sources and plotted against the respective replication rates, r (same symbols as Panel **a**). The RNA content exhibits a linear dependence on the replication rate r as indicated by the line of best-fit given in the plot. In the main text, we determined that the replication rate of particle-associated cells and planktonic cells are respectively $r_s \approx 0.26\,h^{-1}$ and $r_b \approx 0$. The best-fit line then allows us to deduce $R_s : \rho_s \approx 60\,\mu g/(OD \cdot mL)$ and $R_b : \rho_b \approx 50\,\mu g/(OD \cdot mL)$ for these two subpopulations of cells. Together with the result $R_b : R_{total} \approx 0.72$ from Fig. 1d, we obtain $\rho_b : \rho_{total} \approx 0.75 \pm 0.06$. **c)** Direct measurement of RNA content of the different subpopulations of the chitin culture. RNA concentration was measured for samples of the full culture, planktonic cells and on particles only using perchloric acid precipitation.

We observe that the planktonic samples (blue diamonds) were consistently below the full samples (black circles) and similarly to Fig. 1c, we interpret this difference as the biomass accumulating on the surface of the particles. Moreover, the linear increase of RNA concentration with OD in the three samples indicates again that the culture has reached a steady-state. The data points represent the mean value measured and the error bars correspond to the standard deviation across three biological replicates. **d)** To determine the planktonic fraction of the culture (blue diamonds), we took the ratio of the blue diamonds to the black circles in Panel **c**. The error bars are propagated from the standard deviations of the measurements obtained with three biological replicates in panel **c**. This fraction remained constant throughout growth, further establishing that the chitin culture was in a steady-state. The data provides another estimate of the fraction of RNA in the planktonic subpopulation, with $R_b : R_{total} \approx 0.82 \pm 0.1$, which is comparable to the estimate obtained in Fig. 1d using radio-labeling. Using the RNA content described in Panel **b**, the fraction of the planktonic subpopulation is estimated to be $\rho_b : \rho_{total} \approx 0.8 \pm 0.1$, consistent with the estimate of $\rho_b : \rho_{total} \approx 0.75 \pm 0.16$, given above.

a

b

c
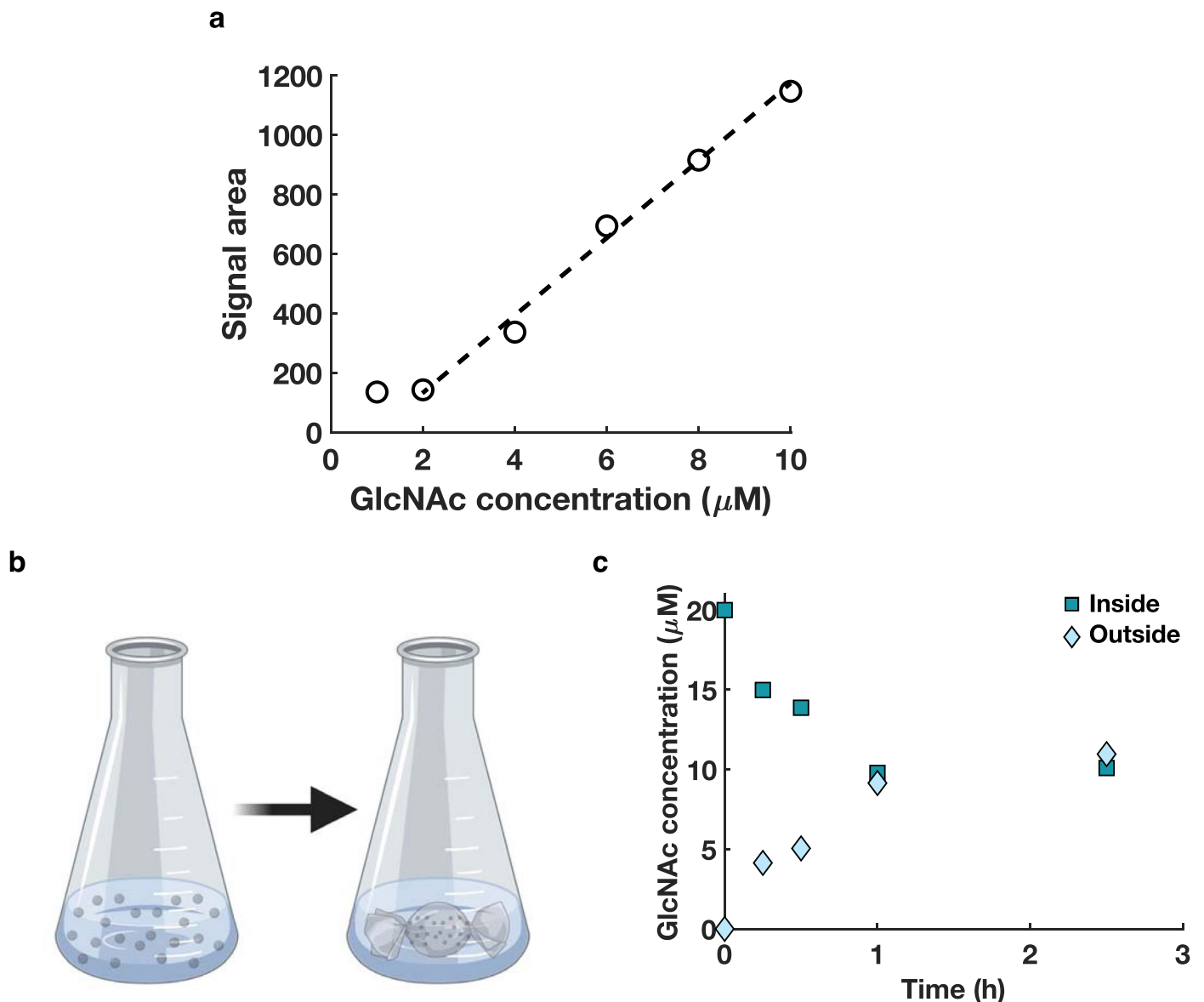
**Extended Data Fig. 2 | Detecting the dynamics of GlcNAc in the media.** **a)** Standard curve showing the detection limit of GlcNAc using HPLC. Several high dilutions of GlcNAc, ranging from $10^{-2}\,\mu M$ were prepared in the minimal media. The samples were passed through a hydrophobic column equipped with a refractive index detector (see HPLC in Methods). Peaks corresponding to GlcNAc eluted between 19.8 and 20.5 minutes, and the total signal area under the curve was determined. The signal area scaled linearly with GlcNAc concentration at the input all the way down to $2\,\mu M$, below which peaks were not detected. Analyzing the supernatant of a growing chitin culture with the same method, yielded an absence of measurable peak, indicated the GlcNAc concentration in the supernatant is below $2\,\mu M$, the detection limit of the HPLC. **b)** Illustration of the dialysis setup in Fig. 2c-d. Chitin particles were separated from planktonic cells in the middle of exponential growth. Chitin particles were resuspended in the same volume of fresh media without particles and placed inside a dialysis bag

with a 14kDa molecular weight cutoff. This pore size means that small molecules such as GlcNAc can exchange but not enzymes, cells nor chitin particles. The dialysis bag was inserted into a flask and the planktonic cells were transferred to the flask, to the exterior of the bag, with equal volumes inside and outside of the dialysis bag. Outside of the dialysis bag, the OD was tracked regularly over a time period of 30 hours, while inside of the bag only the initial and final ODs were recorded due to the difficulty of handling the dialysis tubing. **c)** 10mL of cell-less media with $20\,\mu M$ of GlcNAc was placed in a dialysis bag and incubated with the same volume of media without GlcNAc outside of the bag. The concentrations start equilibrating immediately after the start of the experiment, and reach their equilibrium value by 1h. This indicates that with the full chitin culture in Fig. 2c-d, a low concentration of GlcNAc generated inside the bag can freely exchange between the interior and exterior of the bag if not taken up by cells inside the bag.
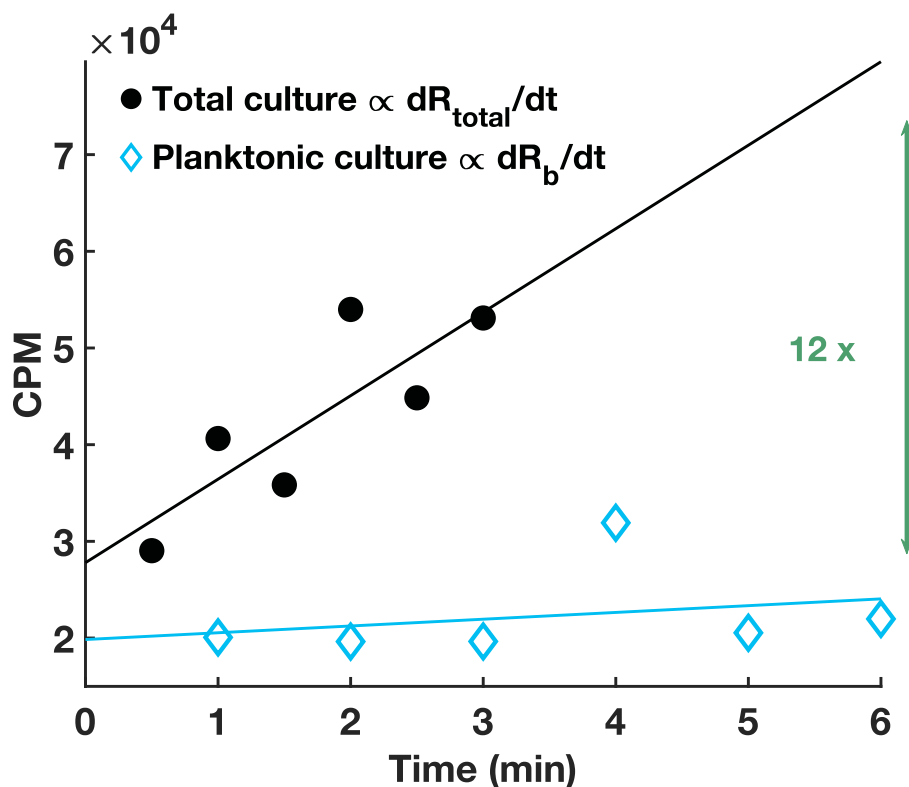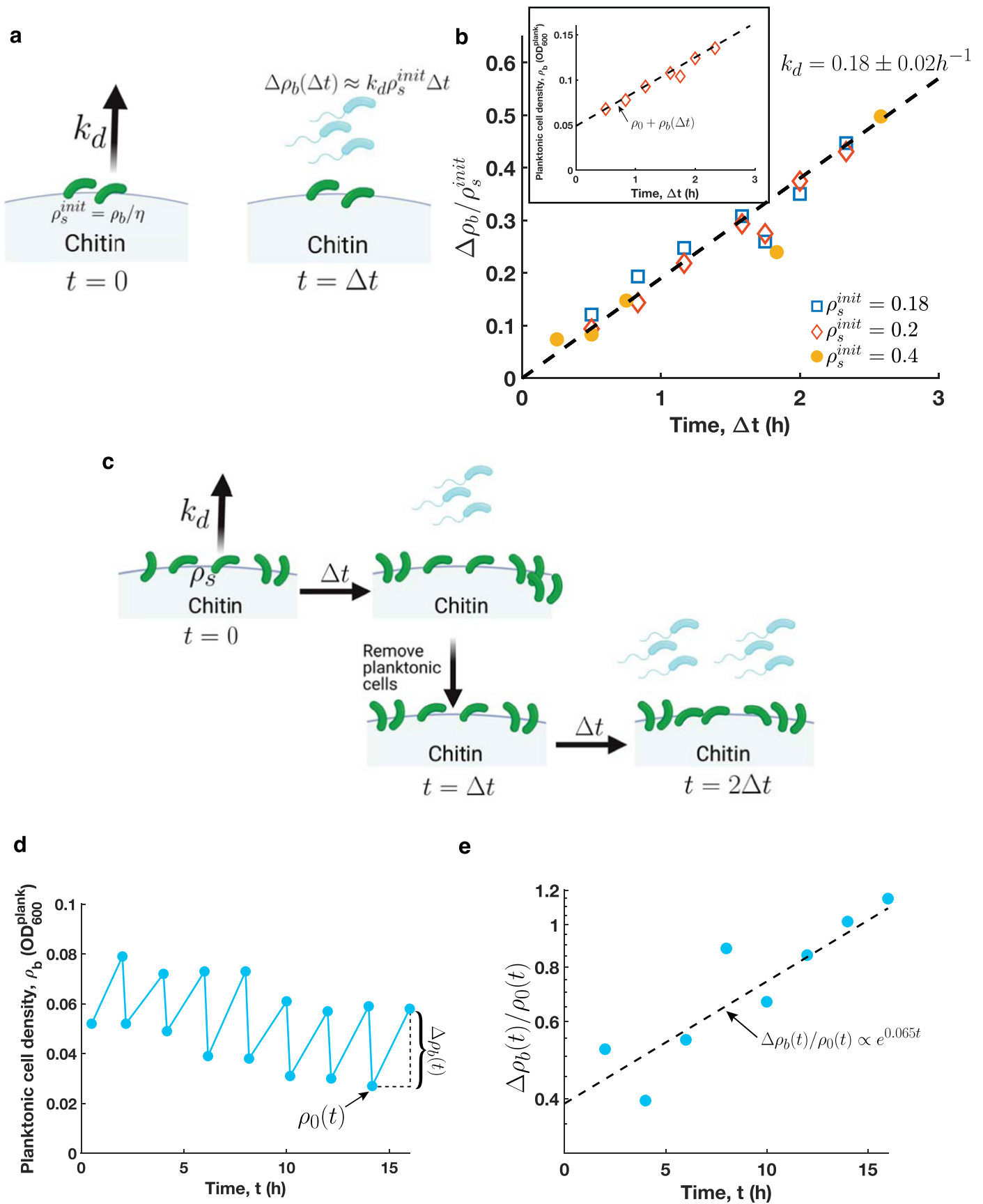
Extended Data Fig. 3 | Instantaneous RNA synthesis rate measurements in the chitin culture. From an exponentially increasing chitin culture at $OD_{600}^{plank} \approx 0.3$, samples of the full culture (including chitin particles and planktonic cells) were compared to samples containing planktonic cells only. The instantaneous RNA synthesis rate, a proxy for the cells' metabolic rate, was measured in both samples by pulsing ^{3}H-Uridine and immediately tracking its incorporation into the total culture and planktonic culture (see RNA synthesis rate in Methods). The plot shows the radioactivity reading as a function of time. The solid lines are linear best fits to the data and their slope represents the metabolic rate in each sample. Specifically let $A_{total} = r_s \rho_s + r_b \rho_b$ be the metabolic rate of the full culture and $A_b = r_b \rho_b$ be the metabolic rate of the planktonic fraction. The result $A_{total}/A_b \approx 12$ indicates that the particle-associated cells were the main contributor to RNA synthesis (and hence cell replication) even though they comprised a minority of the biomass as was determined in Fig. 1 and Extended Data Fig. 1. The replication rates on and off the particles can be compared by taking the ratio A_{total}/A_b and expressing r_b given its contribution to the total biomass: $r_b = (r_s (\rho_{total}/\rho_b - 1))/(A_{total}/A_b - 1) = r_s/33$. Given the estimate of $r_s = 0.26\,h^{-1}$ (main text), this indicates that $r_b \approx 0.008\,h^{-1} \ll \lambda$, making r_b practically negligible.

a

b

c

d
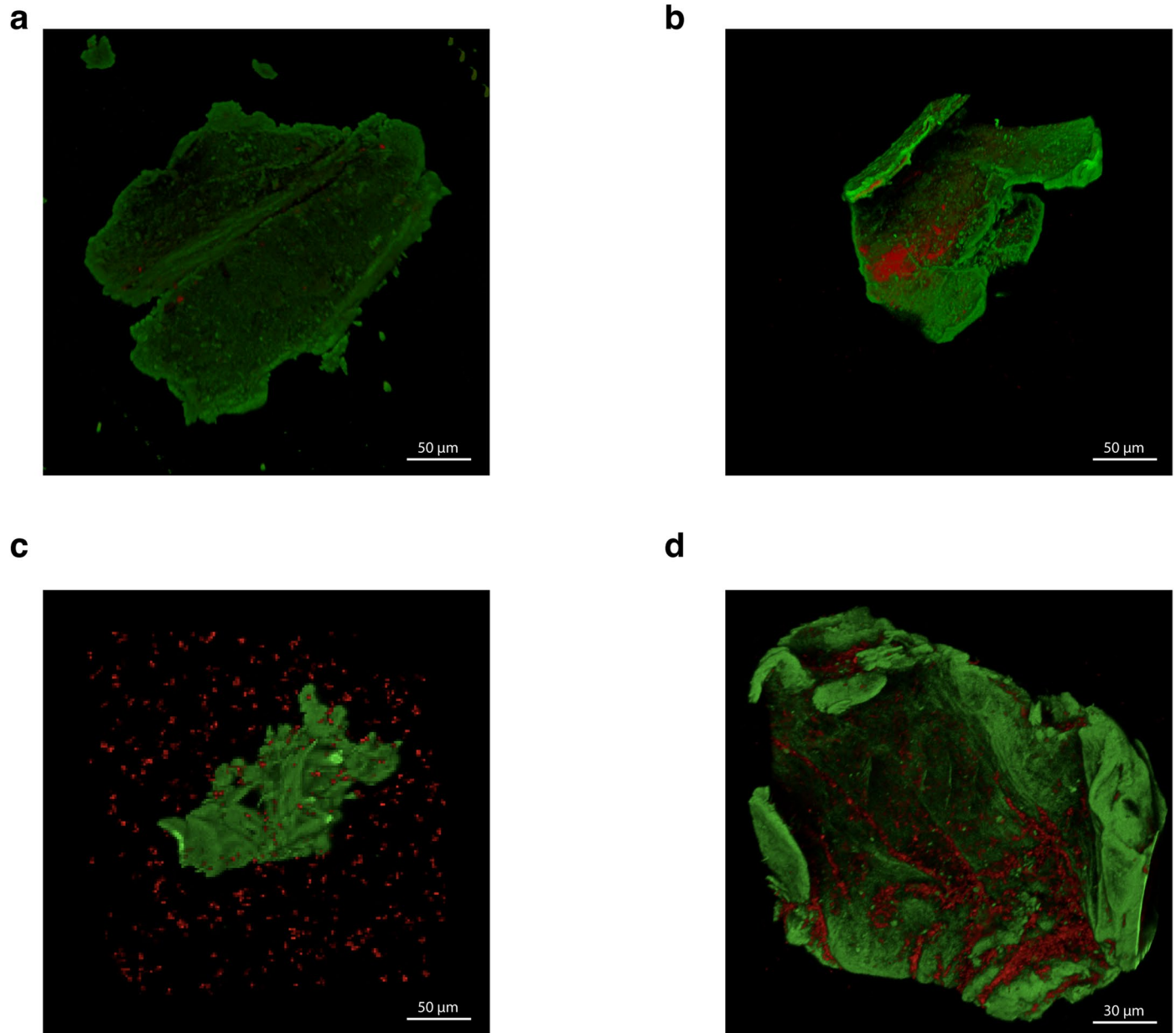
Extended Data Fig. 4 | Microscopy images of chitin particles from growing cultures. Samples were incubated with two fluorescent dyes: FITC-WGA, here shown in the green channel and FM 4-64, a cell membrane dye, shown in the red channel, and fixed with glutaraldehyde. Imaging of the samples was done in custom-built chambers (see microscopy in Methods) under a confocal microscope with 40x magnification. Sample representative images were chosen but microscopy sessions were performed to image 10-50 particles per sample, which all showed similar colonization trends. **a)** Sterile chitin flake incubated with both dyes. FITC-WGA specifically binds to chitin particles, though some FM 4-64 can also be seen in the background. **b)** Chitin particles were isolated from an exponentially increasing chitin culture at $OD_{600}^{plank} = 0.04$ and resuspended in fresh media. Red (membrane dyed) cells can be seen to bind to chitin and form microcolonies. **c)** A sample including both planktonic cells and chitin particles from an exponentially increasing chitin culture at $OD_{600}^{plank} = 0.4$. Consistent with bulk measurements, more planktonic cells are observed than surface-associated cells. **d)** From the same growing culture as in Panel c, chitin particles were isolated and resuspended in fresh media to remove planktonic cells. In both c) and d), the surface of particles is not saturated with cells even at this moderately high OD. This suggests that cell detachment from particles is not a result of a 'space limitation' on the particle surface.

a

$$k_d$$

$$\rho_s^{init} = \rho_b/\eta$$

Chitin

$$t = 0$$

$$\Delta\rho_b(\Delta t) \approx k_d \rho_s^{init} \Delta t$$

Chitin

$$t = \Delta t$$

b

$$k_d = 0.18 \pm 0.02 h^{-1}$$

$$\rho_0 + \rho_b(\Delta t)$$

Planktonic cell density, ρ_b (OD$_{600}^{plank}$)

Time, Δt (h)

$\rho_s^{init} = 0.18$
$\rho_s^{init} = 0.2$
$\rho_s^{init} = 0.4$

$\Delta\rho_b / \rho_s^{init}$

Time, Δt (h)

c

$$k_d$$

$$\rho_s$$

Chitin

$$t = 0$$

$$\Delta t$$

Chitin

Remove
planktonic
cells

Chitin

$$t = \Delta t$$

$$\Delta t$$

Chitin

$$t = 2\Delta t$$

d

Planktonic cell density, ρ_b (OD$_{600}^{plank}$)

$$\Delta\rho_b(t)$$

$$\rho_0(t)$$

Time, t (h)

e

$\Delta\rho_b(t)/\rho_0(t)$

$$\Delta\rho_b(t)/\rho_0(t) \propto e^{0.065t}$$

Time, t (h)

Extended Data Fig. 5 | See next page for caption.

Extended Data Fig. 5 | 1A01 has a dispersal lifestyle. a) Chitin particles pre-colonized with cells (green cells) were isolated at various time (τ) from an exponentially increasing chitin culture, and resuspended in the same volume of fresh media without chitin particles. The amount of particle-associated cells was estimated using the planktonic OD at the time of particle isolation $\rho_b(\tau)$ and the constant planktonic fraction ρ_b: ρ_{total} obtained in Fig. 1, that is, $\rho_s(\tau) = (\frac{\rho_{total}}{\rho_b} - 1)\rho_b(\tau)$. This is taken as the initial cell density ρ_s^{init} of the resuspended culture. For each resuspended culture, the planktonic OD ($\Delta\rho_b$, giving the density of blue cells) was measured at regular time intervals Δt. The increase in planktonic OD is expected to be linear in time with a rate k_d for some time after resuspension. **b)** Inset: the planktonic OD for one such resuspensions increases linearly starting from a background reading ρ_0, due to the turbidity caused by small chitin particles. The dashed line is the line of best fit to the data with a slope $k_d\rho_s^{init}$. Main: Traces of the planktonic OD ($\Delta\rho_b$) were normalized to the initial amount of cells on the particles (ρ_s^{init}) and plotted as a function of time. The normalized traces collapse on top of one another. The slope of the line of best fit (dashed line) allows an estimate of the detachment rate, with $k_d \approx 0.18 \pm 0.02 h^{-1}$, with the error given by the 95% confidence interval of the fit. **c)** Similarly to Panel **a**, pre-colonized chitin particles from a 10mL exponentially increasing chitin culture were separated and re-suspended into the same volume of fresh media without chitin particles. After a time interval of $\Delta t = 2h$, the planktonic OD increased by an amount $\Delta\rho_b$ as a result of cell detachment and with the rate observed Panel **b**. At this point, the particles were sedimented, and resuspended in the same volume of fresh media without chitin particles. This process, which effectively removed all the planktonic cells and thereby prevented reattachment

(effectively setting the attachment rate $k_a \approx 0$), was repeated 8 times, for a total of 16 hours. **d)** Traces of the planktonic OD as a function of time for successive resuspension cycles. From an initial OD measurement ρ_0, which is the background OD due to the residual turbidity of small chitin particles, we observed an increase in the planktonic OD, $\Delta\rho_b$, after the 2h time cycle. The background OD exhibits a time dependence $\rho_0(t)$ due to the successive removal of small particles in the fractionation process. The data shows that in the absence of planktonic cells, the particle-associated cells alone were able to sustain replication and shedding of new planktonic cells in the duration of our experiments, demonstrating that the planktonic culture is not necessary for the replication of cells on the particles. **e)** From the traces in Panel b, we plot the planktonic increase relative to the background OD as a function of time. The normalization by the dynamic background OD allows to adjust for the loss of small particles and hence of surface-associated cells from the culture during the sedimentation process. The dashed line is obtained by fitting an exponential model to the data, with the growth exponent being $0.065 h^{-1}$. Since the cell detachment rate is proportional to the number of cells on particles, the relative increase in planktonic OD, $\Delta\rho_b(t)/\rho_0(t)$, is thus a proxy for the increase in cell density on the particles. We see that this relative increase in planktonic OD is exponential, and that its rate matches the exponential rate measured in an undisturbed chitin culture, $\lambda \approx 0.06 h^{-1}$ (Fig. 1). Since the rate of exponential increase in the planktonic population is hardly affected by the removal of planktonic cells from the chitin culture, we conclude from the data that the attachment rate $k_a \ll \lambda\rho_s/\rho_b = 0.02 h^{-1}$ is thus negligible compared to other rates in our culture.
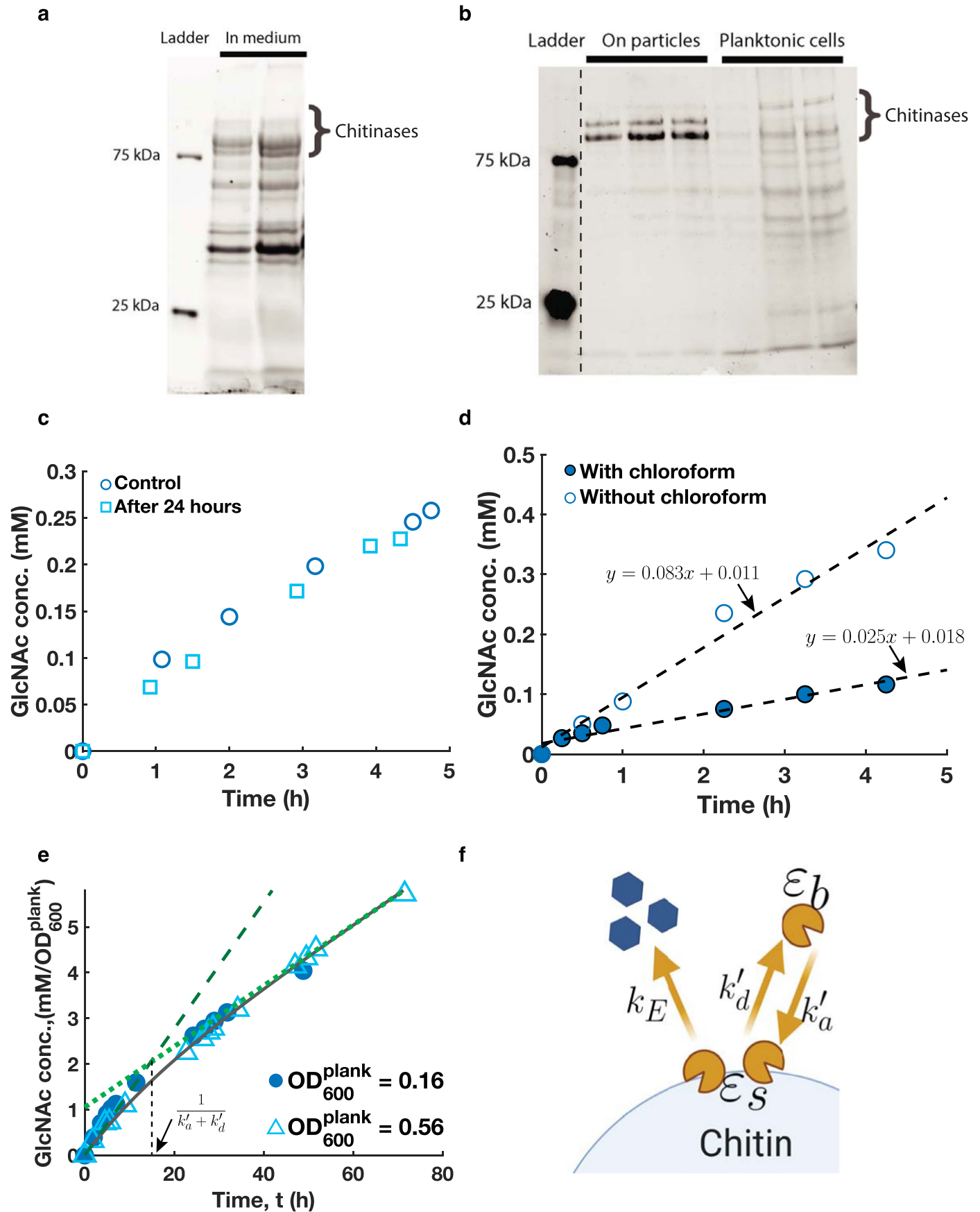
**Extended Data Fig. 6 | See next page for caption.**

Extended Data Fig. 6 | Chitinase activity and properties. a, b) SDS-PAGE gels were run to separate and identify differences in the proteomes of the three fractions of the chitin culture (planktonic cells, particles, and medium after filtering out planktonic cells). To identify the proteins in each band, the bands were excised, solubilized and analyzed using mass spectrometry for identification; see SDS-PAGE in Methods. Bands corresponding to chitinases (with molecular weight ~100kDa) are indicated on the images. Gel image: light intensity and contrast were adjusted. Original gel images are available upon request. Representative gel images were shown but at least three biological replicates were performed for each fraction. **a)** Samples were collected from a steady-state chitin culture at $OD^{plank}_{600} = 0.5, 0.6$ (from left to right). 100 mL of culture was passed through a $0.22\,\mu m$ filter, and the filtrate was concentrated 100-fold using 3kDa concentrators (see fractionation in Methods). The resulting protein mixture was loaded onto the gel. Chitinases are found in the supernatant. See Extended Data Table 1 for the amount quantified. Other unrelated lanes on the same gel were cropped out of the image shown. **b)** Throughout a steady-state chitin culture at multiple planktonic ODs, (at $OD^{plank}_{600} = 0.18, 0.51$ and 0.6 respectively from the left to the right lane), samples were collected and particles separated from planktonic cells. Particles were concentrated 4-fold compared to the volume of planktonic cells to make sure loading amounts were in the same range. After boiling and reducing the proteins (see SDS-PAGE in Methods), they were loaded onto the gel. From the band intensities, it is clear visually that the chitinases are enriched on the particles. This observation is quantitatively confirmed by mass spectrometry, which yields a 5-fold enrichment of chitinases per cell on the particles compared to planktonic cells (see Extended Data Table 1). Gel image: three unrelated lanes between the ladder and the particle samples shown were cropped out from the original image. **c-d)** Proteins from the supernatant of a steady-state chitin culture were collected at $OD^{plank}_{600} \approx 0.5$ and concentrated using the method described above. They were then incubated with fresh chitin flakes and the activity of the enzymes was determined by measuring the GlcNAc concentration in the supernatant at different times using HPLC. **c)** To test the stability of the enzymes, they were resuspended in the same buffer used in our chitin culture. The activity of the enzymes was assayed for similar amounts immediately after their collection (circles) and after being incubated in the same shaking conditions as our culture at 27 °C for 24 hours (squares). This procedure resulted in the same rate of GlcNAc accumulation indicating that the enzymes were stable for the duration assayed. **d)** Because we used chloroform as a way of disabling nutrient uptake in our in situ measurements of enzymatic activity (Fig. 4 and Panel **e**), we independently tested the effect of chloroform on the absolute activity of the chitinases by incubating similar amounts of supernatant enzymes with chitin particles in our culture buffer with and without the addition of chloroform. For each case, we measured the concentration of GlcNAc in the media at regular time intervals (filled and open circles, respectively). The dashed lines represent the linear curves of best fit for the data and the best-fit parameters are indicated on the plots. The ratio of the slopes of the two lines was about 3.3, indicating that the activity of the chitinases enzymes was reduced ~3.3-fold due to chloroform treatment. **e)** Similarly to Fig. 3c, we tracked the accumulation of GlcNAc after treating exponentially growing chitin cultures with chloroform to inhibit carbon uptake by cells in the culture. In this case, GlcNAc accumulation was followed over a longer timescale (3 days) to assess possible changes in chitinase activity, through observing changes in the rate of GlcNAc accumulation. Samples were collected at planktonic ODs of 0.16 (open triangles) and 0.63 (filled circles). The resulting GlcNAc accumulation traces were normalized to the planktonic OD at sampling and we found that the traces collapsed onto each other after normalizing by the initial OD. The reaction was kept at 27 °C and shaking throughout the course of our measurement. The longer timescale of this experiment showed that after 15 hours, there was a change of rate in the accumulation of the GlcNAc concentration (compare dashed to dotted green lines). The second rate was thereafter maintained for ~3 days. This is incompatible with a gradual degradation of chitinases but rather suggests that the system finds a new equilibrium due to the exchange dynamics (attachment and detachment) of the enzymes. **d)** To interpret the data in Panel **e)** and extract the value of the relevant parameters, we formulate the following model governing the GlcNAc accumulation rate. Surface-attached enzymes (ε_s) which produce GlcNAc with a catalytic rate k_E as in Fig. 3 are exchanged with the bulk enzymes (ε_b) with attachment and detachment rates respectively k'_a and k'_d. We plot the best-fit solution for the traces as the solid black line. The full solution of this model can be found in Supplementary Note II. Here we briefly summarize the results: Initially, as explained in Fig. 4b–d, the rate of GlcNAc accumulation is proportional to the enzyme's catalytic rate $s_1 = \kappa_E m_E \varepsilon_s$. At longer times the slope decreases and corresponds to the equilibration of attached and detached enzymes, with $s_2 = {}_E m_E (\varepsilon_s + \varepsilon_b) k'_a / (k'_a + k'_d)$. The ratio of the two slopes is therefore: $s_2 : s_1 = (\varepsilon_s + \varepsilon_b) k'_a / [\varepsilon_s (k'_a + k'_d)]$. The change from one regime to the other occurs at a point $\tau = (k'_a + k'_d)^{-1}$. Thus, with the empirical values of the quantities $s_2 : s_1$ and τ obtained from the data in panel **a**, as well as the ratio $\varepsilon_b : \varepsilon_s$ obtained from Extended Data Table 1 (ratio of the third to the first entry in the last row), we can determine the attachment and detachment rates k'_a and k'_d, with $k'_a = 0.02\,h^{-1}$ and $k'_d = 0.04\,h^{-1}$.
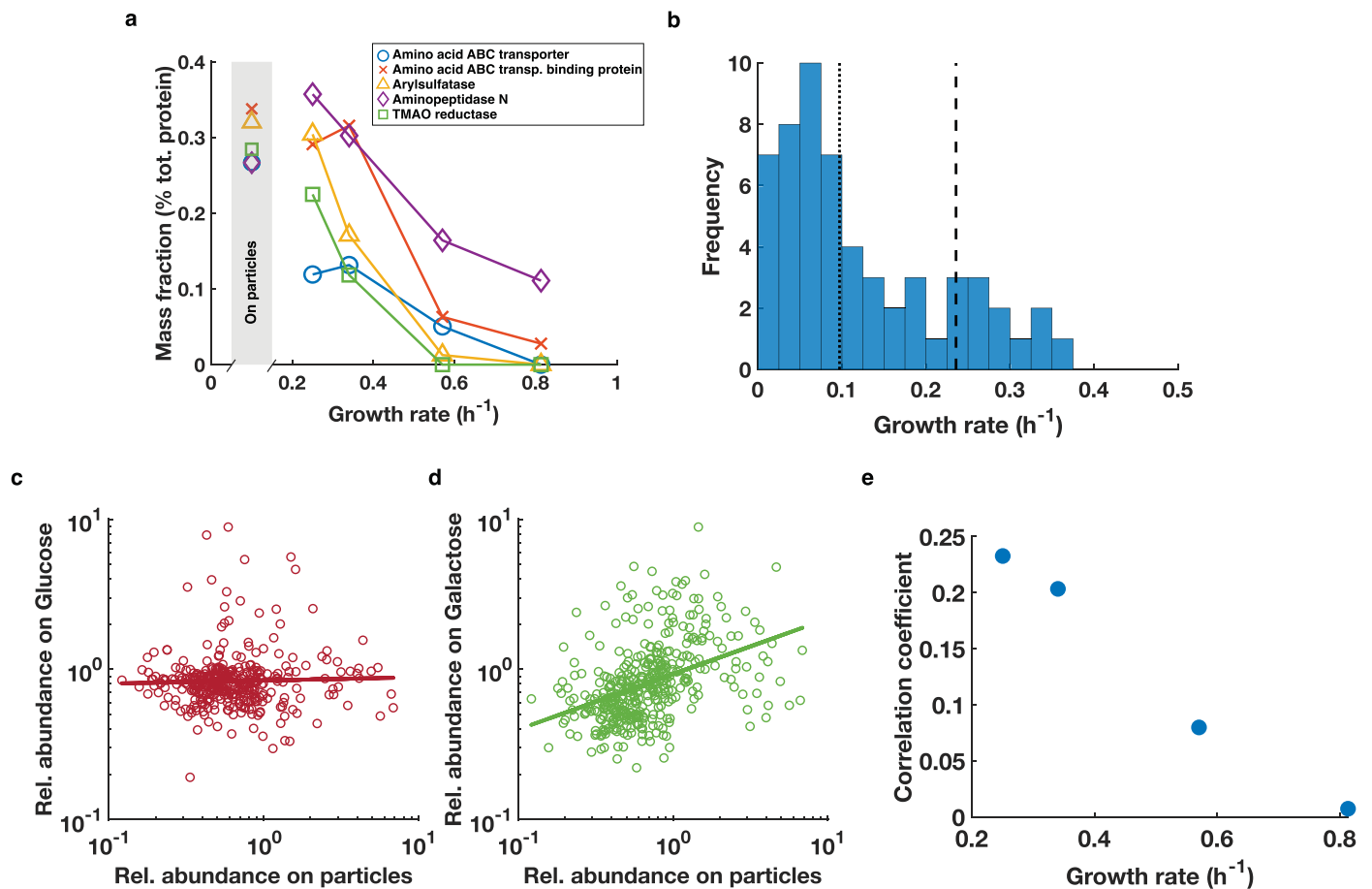
Extended Data Fig. 7 | Analysis of proteomic data. a) Specific examples of proteins whose abundances increased strongly on carbon sources resulting in poor growth. The mass fraction is obtained as the fractional spectral count of these individual proteins in each sample. The x-axis represents the growth rate of the culture under carbon sources of varying quality: Glucose (0.81 h^{-1}), GlcNAc (0.8 h^{-1}), Glucosamine (0.57 h^{-1}), Succinate (0.34 h^{-1}) and Galactose (0.25 h^{-1}). The data in the shaded bar show the mass fraction of these proteins on chitin particles (excluding the chitinases). The abundance of these proteins is more comparable to that on slow growth in poor carbon sources than on fast growth. **b)** Analysis of individual ribosomal proteins. For each ribosomal protein, a linear curve was fitted for its abundance as a function of growth rate using the series described in panel A with varying carbon quality. This linear fit was used as a predictor of the growth rate of surface-associated cells depending on the abundance of individual ribosomal proteins on the particles subtracted of chitinases. The histogram (blue bars) shows the result of the predicted growth rates of surface-associated cells based on each of the 53 ribosomal proteins detected. They yield an average predicted growth rate of 0.23 h^{-1} (dashed vertical line) with the median being even lower, 0.1 h^{-1}, (dotted vertical line). **c-d)** Scatter plots of the relative abundances of proteins from surface-associated cells and cells grown on **c)** glucose and **d)** galactose. Each data point represents the abundance of a protein relative to our ^{15}N labelled standard in both conditions examined. Our standard was composed of a mixture of cells extracted from a fast (glucose) and a medium (succinate) growing condition and injected in equal amount into all of our samples to allow for comparisons between them (see media recipe in Methods). Stronger correlation (0.23) is seen between the proteome of surface-associated cells and cells grown on galactose (poor carbon source giving growth rate of 0.25 h^{-1}), while weaker correlation (0.007) is seen between surface-associated cells and cells grown on glucose (good carbon source giving growth rate of 0.81 h^{-1}). **e)** The correlation coefficient is calculated between the proteome of cells grown in each of the carbon sources studied and that of particle-associated cells as done in panels **c** and **d** except for GlcNAc to avoid biases due to the substrate's nature. Plotting the correlation coefficient with the growth rate of the corresponding carbon source, we see that higher correlation is progressively obtained for slower carbon sources, suggesting that particle-associated cells are carbon-limited.
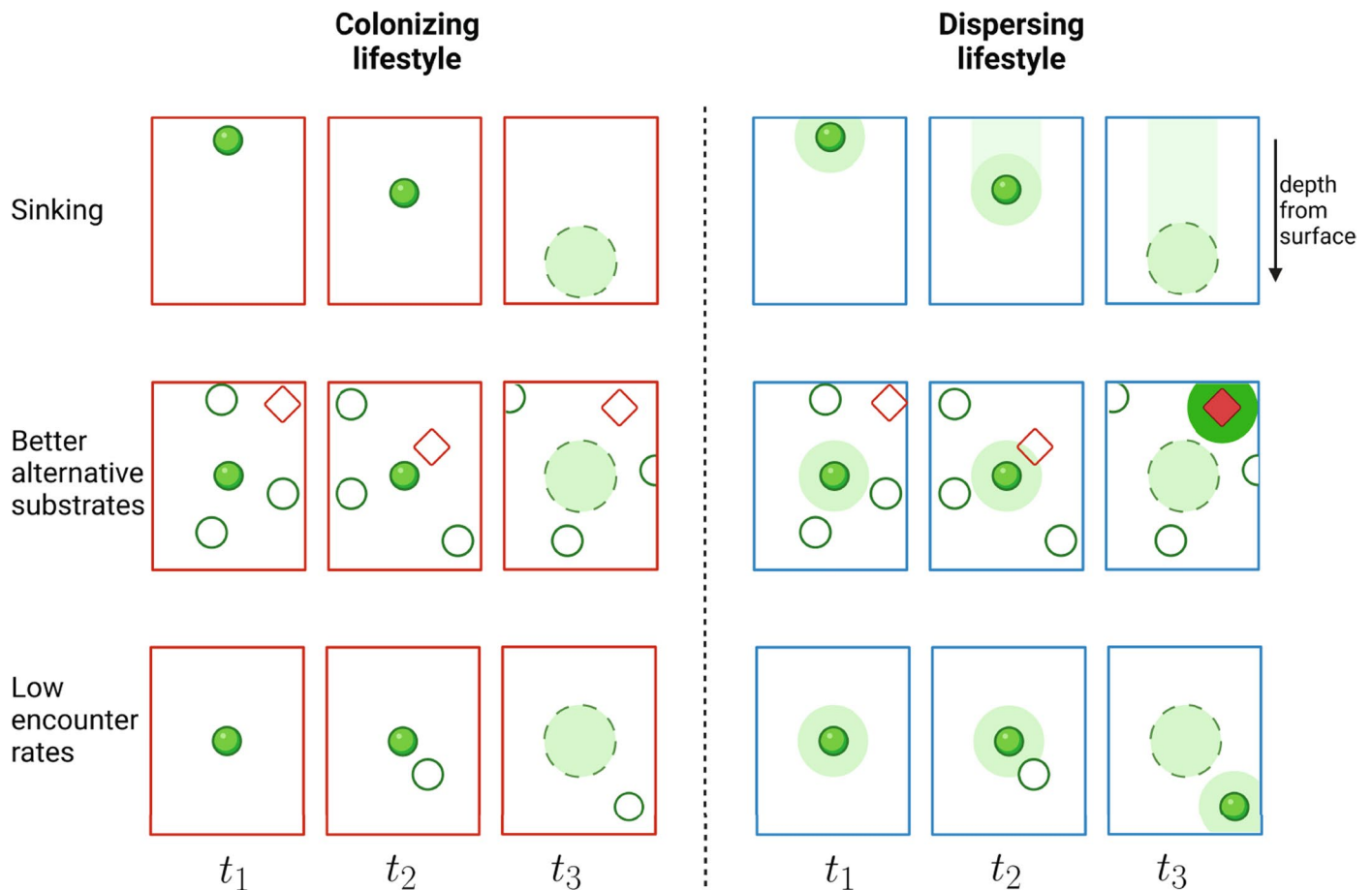
Extended Data Fig. 8 | Possible environmental factors favoring or disfavoring dispersal. Diverse scenarios are presented favoring either the colonizing or the dispersing lifestyle. Briefly, in the colonizing lifestyle, cells do not detach from particles until they are fully consumed, after which all cells are released in a 'burst'. In this case, the 'bursted' population would all die unless one of the cells colonized a fresh particle during the cell lifetime following the burst. In the dispersing lifestyle, a fraction of the population is continuously shed as the particle is being degraded. This allows for cells to seed fresh particles at any time before the particle is fully consumed. For each scenario, the frames from left to right illustrate possible dynamics of the population on and surrounding the particle being degraded. Filled symbols represent colonized particles and the green shade represents planktonic cells. Open symbols represent fresh particles. Diamonds represent a different solid substrate supporting faster growth. **a)** The vertical direction represents depth from the water surface. High detachment rates allow the population to maintain itself along the water column and avoid inho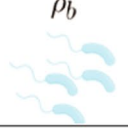spitable depths where oxygen and other factors may become limiting for growth. **b)** A high detachment rate allows the seeding of a particle made of a different substrate (red diamond) providing faster growth. This can be beneficial for certain *Vibrio* sp. species that favor, for example, alginate[50,51]. However, we remark that if detachment reduces the fitness of the population on the existing niche as commonly believed, then exploring alternative resource patches would be more costly. **c)** In situations where the particle density in the environment is low and thus the encounter rate is also low, a high dispersal rate increases the probability of encountering a fresh particle during the 'lifetime' of a colonized particle. If seeding itself is not difficult, this increases the probability of encounter for dispersing cells. On the other hand, if successful seeding is a low probability event while encountering fresh particles is not, then 'bursting' would be more advantageous given the larger number of cells released at burst. This may arise from the requirement on the absolute numbers of cells for the successful colonization of new particles[2], or due to Allee effects arising from other mechanisms.
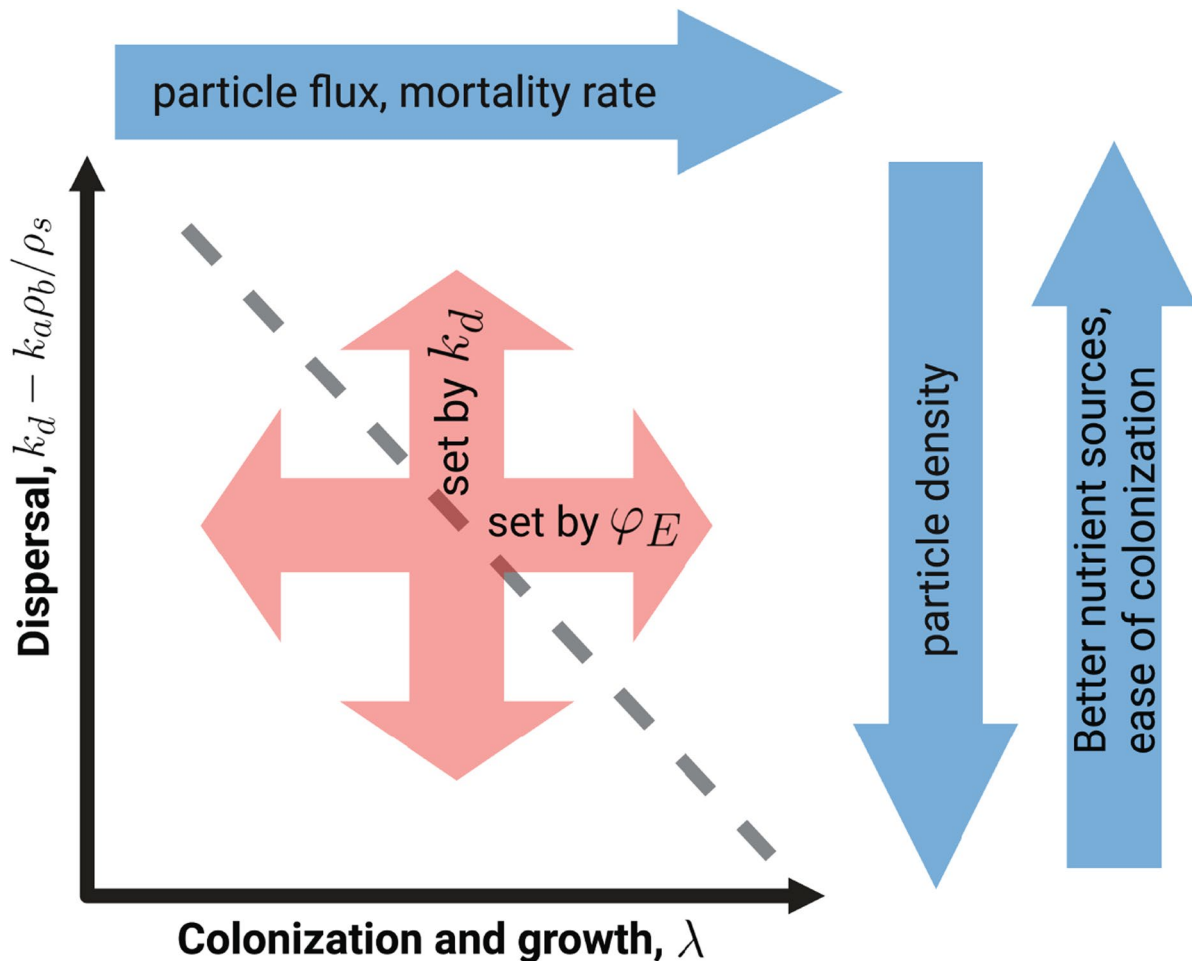
Extended Data Fig. 9 | Cellular and environmental factors determining growth and dispersal. For bacteria such as *Vibrio* sp. 1A01 which release their secreted chitinases, the rate of increase of the population colonized on chitin particles, λ, is decoupled from the rate of detachment from the particles, k_d, circumventing the commonly held trade-off between growth and dispersal, illustrated by the dashed grey line. Instead, growth and dispersal can be separately set molecularly (red arrows), with the population increase rate λ set by φ_E, the allocation towards chitinase synthesis (equation 6). The two molecular parameters k_d and φ_E are in turn dependent on environmental factors such that the population-level fitness, which involves both growth and successful colonization of many particles, increases over long timescales. We speculate

on a number of such environmental factors, represented by the blue arrows. Examples of factors favoring detachment are illustrated in Extended Data Fig. 8. Factors setting the rate of increase of the colonized population may include the rate of particle influx and the rate of mortality on particles (due to grazing, phage killing…) since the survival of the population requires it to grow above the rate of mortality, and as much as allowed by the overall nutrient influx, but not above it to avoid long periods of starvation. We remark that even with growth and dispersal decoupled, an anti-correlation between these two traits may arise if environmental factors favoring one factor also disfavors another. for example, a low particle density resulting from low particle influx would favor slow growth and high detachment.

Extended Data Table 1 | Chitinase abundance in different components of the chitin culture

	ρ_b	ε_b	$\rho_s + \varepsilon_s$	
	Planktonic cells	In medium	On particles	Full culture
Cellular Protein amount $\mu g/(OD_{600}^{plank} \cdot mL)$	**300**[a]	-	100[c]	400[d]
Total protein $\mu g/(OD_{600}^{plank} \cdot mL)$	**300**[a]	**15-30**[b]	125[f]	440-455[i]
Chitinase fraction in sample	**1.6%**[e]	**24%**[e]	**20%**[e]	7.5-8.1%[j]
Chitinase amount $\mu g/(OD_{600}^{plank} \cdot mL)$	4.8[g]	3.6-7.2[g]	25[g]	33-37[h]

Planktonic cells and particles were separated using the sedimentation method described in Fig. 1a and the supernatant was obtained after passage of the entire culture through a 0.2 μm pore size filter and subsequent concentration through a 3 kDa concentrator. See details in Methods. Numbers in bold were directly measured while plain numbers were computed. [a]The protein amount in planktonic cells M_{ρ_b} was measured using the biuret assay. [b]The protein amount in the medium was determined by the biuret assay in the concentrated supernatant (see protein measurement in Methods). [c]The cellular protein amount on particles M_{ρ_s} was computed using the ratio $\eta_b = \frac{M_{\rho_b}}{M_{\rho_b} + M_{\rho_s}}$ found in Fig. 1, with $M_{\rho_s} = \frac{1-\eta_b}{\eta_b} M_{\rho_b} \approx \frac{1}{3} M_{\rho_b}$. [d]The total cellular protein amount is $M_{\rho_b} + M_{\rho_s}$. [e]The chitinase fraction was determined as the sum of chitinase spectral counts (called A0A2G1AS61, A0A2G1AX49 and A0A2G1AVJ7 in the UniProt database, see Supplementary Table 3) divided by the total spectral counts in each sample. We refer to this fraction on the particles as f_s, in planktonic cells as f_b and in the medium as f_m. In particular, $f_s = M_{\varepsilon_s}/(M_{\rho_s} + M_{\varepsilon_s})$. [f]The total amount of proteins (including cellular proteins and chitinases) on the particles $M_{\rho_s} + M_{\varepsilon_s} = \frac{M_{\rho_s}}{1-f_s}$. [g]The chitinase amount in each column is computed as the product of the entries of the second and third row in each column. [h]The total chitinase amount is the sum of left 3 entries of the last row. [i]The total protein amount in the entire chitin culture M_{total} is the sum of the left 3 entries of 2nd row. [j]The chitinase fraction in the total culture is the ratio of the entries of the 4th and 2nd row of the last column.

nature portfolio

Corresponding author(s): Terence Hwa

Last updated by author(s): Jun 19, 2023

Reporting Summary

Nature Portfolio wishes to improve the reproducibility of the work that we publish. This form provides structure for consistency and transparency in reporting. For further information on Nature Portfolio policies, see our Editorial Policies and the Editorial Policy Checklist.

Statistics

For all statistical analyses, confirm that the following items are present in the figure legend, table legend, main text, or Methods section.

n/a	Confirmed	
☐	☒	The exact sample size (*n*) for each experimental group/condition, given as a discrete number and unit of measurement
☐	☒	A statement on whether measurements were taken from distinct samples or whether the same sample was measured repeatedly
☒	☐	The statistical test(s) used AND whether they are one- or two-sided *Only common tests should be described solely by name; describe more complex techniques in the Methods section.*
☒	☐	A description of all covariates tested
☒	☐	A description of any assumptions or corrections, such as tests of normality and adjustment for multiple comparisons
☐	☒	A full description of the statistical parameters including central tendency (e.g. means) or other basic estimates (e.g. regression coefficient) AND variation (e.g. standard deviation) or associated estimates of uncertainty (e.g. confidence intervals)
☒	☐	For null hypothesis testing, the test statistic (e.g. *F*, *t*, *r*) with confidence intervals, effect sizes, degrees of freedom and *P* value noted *Give P values as exact values whenever suitable.*
☒	☐	For Bayesian analysis, information on the choice of priors and Markov chain Monte Carlo settings
☒	☐	For hierarchical and complex designs, identification of the appropriate level for tests and full reporting of outcomes
☒	☐	Estimates of effect sizes (e.g. Cohen's *d*, Pearson's *r*), indicating how they were calculated

Our web collection on statistics for biologists contains articles on many of the points above.

Software and code

Policy information about availability of computer code

Data collection	Proteomic measurements were performed on a AB Sciex 5600 TripleTOF.
Data analysis	Data analysis was performed according to Hui et al. (2015).

For manuscripts utilizing custom algorithms or software that are central to the research but not yet described in published literature, software must be made available to editors and reviewers. We strongly encourage code deposition in a community repository (e.g. GitHub). See the Nature Portfolio guidelines for submitting code & software for further information.

Data

Policy information about availability of data

All manuscripts must include a data availability statement. This statement should provide the following information, where applicable:
- Accession codes, unique identifiers, or web links for publicly available datasets
- A description of any restrictions on data availability
- For clinical datasets or third party data, please ensure that the statement adheres to our policy

The mass spectrometry proteomics data have been deposited to the ProteomeXchange Consortium (Vizcaíno et al, 2014) via the UCSD MassIVE partner repository with the dataset identifier PXD034003. Summary tables including both absolute and relative quantitation as well as functional grouping can be found in Tables S2 and S3. Peptides were searched and identified using X!Tandem (Alanine version) against the UniProt Vibrio sp. 1A01 database (organism ID 314742). All other data that support the findings of this study are available from the corresponding author upon request. Source data where relevant has been provided to

the editor and any additional data (in particular physiological measurements and their replicates) can be shared upon request.

Human research participants

Policy information about studies involving human research participants and Sex and Gender in Research.

Reporting on sex and gender	N/A
Population characteristics	N/A
Recruitment	N/A
Ethics oversight	N/A

Note that full information on the approval of the study protocol must also be provided in the manuscript.

Field-specific reporting

Please select the one below that is the best fit for your research. If you are not sure, read the appropriate sections before making your selection.

☒ Life sciences   ☐ Behavioural & social sciences   ☐ Ecological, evolutionary & environmental sciences

For a reference copy of the document with all sections, see nature.com/documents/nr-reporting-summary-flat.pdf

Life sciences study design

All studies must disclose on these points even when the disclosure is negative.

Sample size	For proteomic measurements, the sample size was chosen to obtain enough peptides for mass spectrometer detection (~50ug or proteins). For growth measurements, sample size was chosen so that the growth rate or lag time could be quantified and discriminated from condition to condition.
Data exclusions	No data were excluded from the study
Replication	Three technical replicates were performed for proteomic measurements, and showed no significant variability. All technical replicates were successfully run. For growth and other measurements in this study, independent replicates are done for key experiments as detailed in Methods, Figure legends and Supplementary Table S1.
Randomization	This is not relevant to our study as we characterized a single organism. The phenomenological nature of our study does not permit for randomizing samples as we were characterizing populations of single organisms.
Blinding	This is not relevant to our study as we characterized a single organism. The phenomenological nature of our study does not permit for randomizing samples as we were characterizing populations of single organisms.

Reporting for specific materials, systems and methods

We require information from authors about some types of materials, experimental systems and methods used in many studies. Here, indicate whether each material, system or method listed is relevant to your study. If you are not sure if a list item applies to your research, read the appropriate section before selecting a response.

Materials & experimental systems

n/a	Involved in the study
☒ ☐	Antibodies
☒ ☐	Eukaryotic cell lines
☒ ☐	Palaeontology and archaeology
☒ ☐	Animals and other organisms
☒ ☐	Clinical data
☒ ☐	Dual use research of concern

Methods

n/a	Involved in the study
☒ ☐	ChIP-seq
☒ ☐	Flow cytometry
☒ ☐	MRI-based neuroimaging

Inherited chitinases enable sustained growth and rapid dispersal of bacteria from chitin particles

In the format provided by the
authors and unedited

SUPPLEMENTARY TABLES   2

SUPPLEMENTARY NOTES   4

SUPPLEMENTARY REFERENCES   25

SUPPLEMENTARY TABLE

Parameter	Unit	Notation	Value	Source
Max. replication rate on GlcNAc	h^{-1}	r_{max}	0.8 ± 0.05	Fig. 1b
Population growth rate on chitin	h^{-1}	λ	0.06 ± 0.01	Fig. 1b
Density of planktonic cells	$OD_{600}^{plank} \approx 10^9 \; cells/mL$	ρ_b	various	Supp. Ref. [1]
Fraction of planktonic cells	--	η_b	0.75 ± 0.06	Fig. 1c
Number of particle-associated cells per culture volume	OD_{600}^{plank} equivalent	ρ_s	various	$\rho_b \cdot (1 - \eta_b)/\eta_b$
Rate of cell detach. from chitin	h^{-1}	k_d	0.18 ± 0.02	Ext. Data Fig. 5b
Cell Yield of GlcNAc	OD_{600}^{plank}/mM	Y	0.16	Supp. Ref. [1]
Cell dry mass	$\mu g/ml/OD_{600}^{plank}$	m_{cell}	575 ± 25	Supp. Ref. [2]
Cell protein mass	$\mu g/ml/OD_{600}^{plank}$	m_P	300 ± 30	Ext. Data Table 1
Molecular weight of chitinase	kDa	m_E	100	Ext. Data Fig. 6
Protein yield of GlcNAc	$\mu g/mL/mM$	Y_P	48 ± 5	$Y \cdot m_P$
Biomass yield of GlcNAc	$\mu g/mL/mM$	Y_b	92 ± 4	$Y \cdot m_{cell}$
Total cellular protein on particles	$\mu g/ml/OD_{600}^{plank}$	$\rho_s m_P/\rho_b$	100	$m_P(1 - \eta_b)/\eta_b$
Mass fraction of chitinase amongst all proteins on particle	%	f_s	20	Ext. Data Table 1
Mass fraction of chitinase on particles among all chitinases	%	f_E	71 ± 5	footnote a
Chitinase amount on particle	$\mu g/ml/OD_{600}^{plank}$	$m_E \varepsilon_s/\rho_b$	25	$\dfrac{\rho_s m_P}{\rho_b} \cdot \dfrac{f_s}{1 - f_s}$
GlcNAc production flux	$mM/h/OD_{600}^{plank}$	J_n/ρ_b	0.6	footnote b
Specific chitinase activity	$nmol/\mu g/h$	κ_E	24 ± 5	Fig. 3
Fraction of biomass production towards chitinases on particles	%	φ_E	3 ± 0.2	footnote c
Fraction of total proteome that are chitinases	%	χ_E	4.9 ± 0.5	footnote d
Fraction of biomass production towards all chitinases	%	$\varphi_{E,tot}$	4.2 ± 0.3	φ_E/f_E
Max. allocation for cell growth	%	φ_{max}	34 ± 4	footnote e

Table S1: Summary of parameters and their values. We summarize the key cellular and molecular quantities obtained in this work, by either direct measurement (indicated by the Figure or Table where the result is derived), or indirectly from measured quantities (indicated by the relation used to compute them).

a) f_E is the ratio of the amount of chitinase found on particle to the total amount of chitinase in the culture; values of the latter are given as the 3rd and 4th entries of the last row of Extended Data Table 1.

b) We can check that the GlcNAc production flux indeed supports the growth of the entire culture such that $J_n Y_b = \lambda \big(m_{cell}(\rho_b + \rho_s) + m_E(\varepsilon_b + \varepsilon_s) \big) \approx \lambda(m_{cell}(\rho_b + \rho_s))$. Solving for the growth rate, we find $\lambda = \frac{J_n}{\rho_b} \eta_b Y_b = 0.07 h^{-1}$, quantitatively corresponding to the observed growth rate.

c) φ_E is defined as the fraction of the total nutrient flux that goes towards chitinase synthesis, i.e., $\varphi_E \equiv \frac{J_E}{J_{rep} + J_E} = \frac{m_E \varepsilon_s}{(\rho_b + \rho_s)m_{cell} + m_E \varepsilon_s}$. It can be rewritten as $\varphi_E = \frac{m_E \varepsilon_s / \rho_b}{m_{cell} \cdot (\rho_b + \rho_s)/\rho_b + m_E \varepsilon_s / \rho_b}$ and determined using the parameter values listed above.

d) χ_E is defined as the fraction of proteins in the culture that are chitinases such that $\chi_E \equiv m_E \varepsilon_s / \big((\rho_s + \rho_b) \cdot m_P + m_E \varepsilon_s \big)$. It can be related to the nutrient flux fraction φ_E from $\chi_E = \varphi_E / [b + (1 - b)\varphi_E]$ where $b = m_P / m_{cell}$.

e) φ_{max} is the maximum fraction of the nutrient flux dedicated to the synthesis of proteins necessary for growth in the fastest growth condition. We first estimated χ_{max} by observing that at the fastest growth rate $\chi_{max} \approx 50\%$ (since the translational apparatus is 18%, enzyme biosynthesis 17%, transporters 5%, glycolytic enzymes 7% and TCA enzymes 4% (see Summary sheet in Table S3)). We next converted this quantity from a protein fraction to a nutrient flux fraction φ_{max} since $\varphi_{max} = b\chi_{max} / [1 - (1 - b)\chi_{max}]$ where $b = m_P / m_{cell}$.

SUPPLEMENTARY NOTES

I-A population-level model for chitin degradation
    In this section we present the most general framework for describing the processes that lead to chitin degradation at the population level, including both cell and enzyme dynamics. After describing this framework, we will examine the properties of two specific bacterial strategies: one in which enzymes are secreted and released extra-cellularly and another in which enzymes remain attached to the cell surface.

1- <u>General population-level model</u>
    Vibrio sp. 1A01 cells are grown in a minimal medium with chitin flakes as their sole source of Carbon and Nitrogen. We refer to planktonic or **b**ulk components with the subscript b and to **s**urface associated components with the subscript s.
    The total volume of the culture is V and the amount of chitin in the culture is described by the weight density ϕ_w. Given chitin's density $d_c = 1.4 \ g/mL$, the number density of chitin particles is $\phi_v = \phi_w/d_c$. For a chitin particle of volume v_p, the number of chitin particles in the culture is: $N_c = \phi_v V/v_p$. Hence the number density of chitin particles is $\rho_c = N_c/V = \phi_v/v_p$. The particle volume v_p depends on the shape of the particles, which we approximate as spheres of radius R_0 such that $v_p = 4/3\pi R_0^3$.
    We define cellular and enzymatic variables in the chitin culture:
- Let N_b be the total number of cells in the bulk. $\rho_b = N_b/V$ is the cell density in the bulk.
- Let N_s be the total number of cells associated with the surface of the chitin particles. $\rho_s = N_s/V$ is the surface-associated cell density. We note that these also include cells that are in the immediate vicinity of particles, in the "chitosphere", as we explain more clearly in Supp. Note III. The number of cells per particle is ρ_s/ρ_c.
- Let N_{ε_b} be the number of chitinases in the bulk. $\varepsilon_b = N_{\varepsilon_b}/V$ is the chitinase density in the bulk.
- Let N_{ε_s} be the number of chitinases associated with the surface of the chitin particles. $\varepsilon_s = N_{\varepsilon_s}/V$ is the chitinase density in the bulk. The number of enzymes per particle is ε_s/ρ_c.
- n is the GlcNAc concentration on the surface of particles.

With these components, the most general model at the population level is:

$$\frac{d\rho_b}{dt} = k_d \rho_s + (r_b - k_a)\rho_b \tag{S1}$$

$$\frac{d\rho_s}{dt} = (r_s - k_d)\rho_s + k_a \rho_b \tag{S2}$$

$$\frac{d\varepsilon_b}{dt} = \beta_b \rho_b + k'_d \varepsilon_s - k'_a \varepsilon_b \tag{S3}$$

$$\frac{d\varepsilon_s}{dt} = \beta_s \rho_s - k'_d \varepsilon_s + k'_a \varepsilon_b \tag{S4}$$

$$\frac{dn}{dt} = k_E \varepsilon_s - \mu \rho_s - j_D \qquad \text{(S5)}$$

Where:
- k_d and k_a are the cell detachment and attachment rates respectively,
- r_b and r_s are the cell replication rates in the bulk and on the surface of the particles respectively,
- k'_d and k'_a are the enzymes' detachment and attachment rates respectively,
- β_b and β_s are the chitinase synthesis rates by the bulk and surface-associated cells respectively,
- μ is the nutrient uptake rate by surface-associated cells,
- k_E is the catalytic rate of the chitinases referred to in the main text as $k_E = \kappa_E m_E$, where κ_E is the catalytic rate per enzyme mass and m_E the enzyme mass,
- j_D is the nutrient loss due to diffusion, referred to in the main text as j_{loss}

Given this system, let's follow the nutrient flux and define a few flux quantities. Let J_n be the total nutrient generation flux in units of mM/h. To ensure flux balance in this closed system, this flux supports the total biomass growth such that $J_n = J_{rep} + J_E + j_{loss}$. J_{rep} is the nutrient flux dedicated to cellular replication and biomass while J_E is the nutrient flux dedicated to chitinase synthesis (see Fig. 3 in Main text). In section III, we argue why j_{loss} can be neglected from this calculation. This is also supported by the experimental observation that planktonic cells aren't replicating (see Fig. 2 in main text). To relate the molecular variables defined in the system above (Eqs. S1-S5) to these fluxes, we consider Y_b as the biomass yield of 1A01 growing on GlcNAc, which acts as a conversion factor between biomass and nutrient concentration.

To ensure flux balance, the total nutrient flux is thus:
$$J_n Y_b = \Sigma_i \left(\dot{\rho}_i + \dot{\varepsilon}_i \right) \qquad \text{(S6)}$$

And the flux going towards chitinase synthesis only:

$$J_E Y_b = \Sigma_i \dot{\varepsilon}_i \qquad \text{(S7)}$$

Similarly to the main text, it is convenient to introduce the quantity φ_E, which describes the fraction of the total nutrient flux going towards chitinase synthesis:

$$\varphi_E \equiv J_E / (J_{rep} + J_E) \qquad \text{(S8)}$$

This fraction of the flux directed to chitinase synthesis is a key control parameter since it describes the cost incurred to cells as a result of chitinase production. If there were no cost associated with chitinase production, the replication rates r_i, would only depend on the nutrient concentration through the Monod form:

$$r_i(n/K) = r_{max} \frac{n/K}{1+n/K}$$

Where:
- r_{max} is the maximal growth rate of 1A01 in minimal media with GlcNAc as the sole carbon source,
- n/K is the nutrient concentration available in units of the Monod constant K.

However, given the necessity of synthesizing chitinases and its potential cost on the proteome of 1A01, we modify this form of the replication rate by referring back to results in Scott et al. (2010)[3]. To complete the description of the system, we introduce the proteomic cost of chitinase synthesis on the replication rate of surface associated cells. For a fixed nutrient level, the replication rate can be expressed as follows:

$$r_i(n/K, \varphi_E) = r_{max} \frac{n/K}{1+n/K} \cdot (1 - \varphi_E/\varphi_{max}) \qquad \text{(S9)}$$

Where:
- φ_{max} is defined as the maximum nutrient flux fraction dedicated to growth (refer to Figure 4B in Scott et al. (2010)).

To intuitively understand the form of this function, we consider two limiting cases. On the one hand if $\varphi_E = 0$, growth is nutrient limited as it would be in a chemostat, the replication rate solely depends on nutrient levels: $r_s(n/K, \varphi_E = 0) = r_{max} \frac{n/K}{1+n/K}$.
On the other hand, for situations in which $\varphi_E \neq 0$, there would be a cost to chitinase production with a maximal effect when $\varphi_E = \varphi_{max}$, at which point the cells can no longer replicate since all of their available biomass is divested from biosynthetic proteins and ribosomes and goes towards chitinase production. In this case: $r_i(n/K, \varphi_E = \varphi_{max}) = 0$.

We note that even though here the control parameter φ_E is expressed as a nutrient flux fraction, it can easily be converted to the variables usually used in models including the cost of protein overexpression[4,5]. These models are generally written in terms of proteomic fractions χ_i, since these are the experimentally accessible quantities. In particular, we can write $\chi_i = b\chi/[1 - (1-b)\chi]$ where $b = m_P/m_{cell}$ converts between protein mass and biomass of the cell.

2- <u>Case of secreted chitinases</u>
a- <u>Experimental constraints</u>
Experimental findings allow to constrain the previous model given the measured parameters for the growth *Vibrio sp.* 1A01 on chitin.
In Fig. 1, we demonstrate using several ways that our system is in steady-state, with both the planktonic and particle-associated fraction increasing exponentially at the same exponential rate, λ. We refer to this parameter as the population increase rate.
In Fig. 2, we demonstrate that planktonic cells aren't replicating, (i.e: $r_b = 0$). Moreover, in Extended Data Table 1 we show that their chitinase production is negligible (i.e: $\beta_b = 0$).

Since the planktonic cells aren't replicating this is a strong experimental indication that the diffusive loss term j_{loss} is negligible compared to the other fluxes. Another way to convince ourselves that j_{loss} is negligible in this steady-state is to compare it to the other terms in Eq. S5. The loss term can be modelled as: $j_{loss} = 4\pi D R_0 \rho_c Sh$ where D is the diffusion coefficient and Sh the Sherwood number. On the surface of the particles and at steady-state, ε_s and ρ_s increase exponentially while the diffusion term doesn't. A more complete model which shows that the diffusion loss term decays with a finite screening length is solved in Section III of this note.

In Extended Data Fig. 5 we experimentally determine the value of k_d and establish that k_a is small compared to λ.

These estimates allow to reduce Eq. S1-S5 to this simplified system of equations:

$$\frac{d\rho_b}{dt} = k_d \rho_s \tag{S10}$$

$$\frac{d\rho_s}{dt} = (r_s - k_d)\rho_s \tag{S11}$$

$$\frac{d\varepsilon_b}{dt} = k_d' \varepsilon_s - k_a' \varepsilon_b \tag{S12}$$

$$\frac{d\varepsilon_s}{dt} = \beta_s \rho_s - k_d' \varepsilon_s + k_a' \varepsilon_b \tag{S13}$$

$$\frac{dn}{dt} = k_E \varepsilon_s - \mu \rho_s \tag{S14}$$

The total nutrient flux in units of $[mM/h]$, is $J_n = k_E \varepsilon_s$. Given the system is at steady-state with an exponential rate of increase λ, we solve Eqs. S10-S14 to obtain the following solution:

$$\eta \equiv \rho_b / \rho_s = k_d / \lambda \tag{S15}$$

$$\lambda = r_s(n/K, \varphi_E) - k_d \tag{S16}$$

$$\eta' \equiv \varepsilon_b / \varepsilon_s = k_d' / (\lambda + k_a') \tag{S17}$$

$$\beta_s \rho_s = (\lambda + k_d')\varepsilon_s - k_a' \varepsilon_b \tag{S18}$$

$$k_E \varepsilon_s = J_n \tag{S19}$$

In Figure 1, we measure λ and η. These measurements help estimate r_s.

Experiments in Figures 4 and Extended Data Fig. 6, help determine the enzyme properties k_E, k_a' and k_d' as well as their steady-state repartition η'. We note that in the main text we treat the simpler case in which enzymes automatically attach to particles and don't detach from them. This corresponds to the case where $k_d' = 0$ and $\varepsilon_b = 0$.

Using the definitions in Eqs. S6-S7, as well as the steady-state solution, we express the various nutrient fluxes as:

$$J_n Y_b = r_s \rho_s + \beta_s \rho_s \tag{S20}$$
$$= \lambda(\rho_b + \rho_s + \varepsilon_b + \varepsilon_s) \tag{S21}$$

And

$$J_E Y_b = \beta_s \rho_s \tag{S22}$$
$$= \lambda(\varepsilon_b + \varepsilon_s) \tag{S23}$$

Which leads to the steady-state expression for φ_E using its definition in Eq.S8:

$$\varphi_E = \frac{\varepsilon_b + \varepsilon_s}{\rho_b + \rho_s + \varepsilon_b + \varepsilon_s} \qquad (S24)$$

The two key control parameters that cells can control within the timescale of our experiment (i.e: as a result of gene regulation) are φ_E and k_d. On the other hand, enzyme parameters such as k_E, k_d' and k_a' are dictated by the genetic sequences available to 1A01 and can only change on longer time scales and as a result of sequence evolution. Below, we examine the effect of changing these two key parameters on the properties of the steady-state solution described here.

b- *Examining the effect of φ_E and k_d on the system*
Our goal in this section is to examine the dependence of λ on the control parameters φ_E and k_d.

Subtracting Eqs. S20 and S22 and expressing J_n as in Eq. S19 allows to find the replication rate r_s as a function of the control parameters:

$$Y_b(1 - \varphi_E)J_n = r_s\rho_s \qquad (S25)$$
$$\rightarrow r_s = Y_b(1 - \varphi_E)k_E\varepsilon_s/\rho_s \qquad (S26)$$

Thus, given Eq. S16,

$$\lambda = (1 - \varphi_E)\kappa_E m_E Y_b \varepsilon_s/\rho_s - k_d \qquad (S27)$$

Rearranging this expression for $m_E\varepsilon_s/\rho_s$ and plugging the result into the steady-state expression for φ_E, in Eq. S20 we get:

$$\varphi_E = \left(\frac{1+\eta'}{1+\eta}\varepsilon_s/\rho_s\right)/\left(1 + \frac{1+\eta'}{1+\eta}\varepsilon_s/\rho_s\right) \qquad (S28)$$

Using Eqs. S15 and S17, $\frac{1+\eta'}{(1+\eta)}\varepsilon_s/\rho_s$ can be written as:

$$\frac{1+\eta'}{(1+\eta)}\varepsilon_s/\rho_s = \frac{\lambda + k_{a'} + k_{d'}}{\lambda + k_{a'}}\frac{\lambda}{(1-\varphi_E)\kappa_E Y_b} \qquad (S29)$$

Thereby cancelling the k_d dependence of φ_E:

$$\varphi_E = \frac{\dfrac{\lambda + k_a' + k_d'}{\lambda + k_a'}\dfrac{\lambda}{(1 - \varphi_E)k_E Y_b}}{1 + \dfrac{\lambda + k_a' + k_d'}{\lambda + k_a'}\dfrac{\lambda}{(1 - \varphi_E)k_E Y_b}}$$

Rearranging for λ in the previous equation, we have:
$$\lambda^2 + (k_a' + k_d' - \kappa_E Y_b \varphi_E)\lambda - k_a'\kappa_E Y_b \varphi_E = 0$$
Now solving this quadratic form, we find $\lambda(\varphi_E)$:

$$\to \lambda(\varphi_E) = \frac{1}{2}\left(k_E Y_b \varphi_E - (k'_a + k'_d) + \sqrt{(k'_a + k'_d - k_E Y_b \varphi_E)^2 + 4k'_a k_E Y_b \varphi_E} \right) \text{ (S30)}$$

This analysis indicates that surprisingly the exponential population increase rate, λ, is independent of the cell detachment rate k_d while it has a non-trivial dependence on the allocation towards chitinase synthesis φ_E.

To further understand this behavior, let's first consider the simplifying case in which $k'_a = 0$. This more closely resembles the situation that these types of system may encounter in the ocean since any detached enzymes would easily diffuse away. In this case, Eq. S30 becomes:

$$\begin{aligned}\lambda(\varphi_E) &= (k_E Y_b \varphi_E - k'_d)/2 + | \, k'_d - \kappa_E Y_b \varphi_E| \\ &= \begin{cases} 0 & \text{for } k'_d > k_E Y_b \varphi_E \\ k_E Y_b \varphi_E - k'_d & \text{for } k'_d < k_E Y_b \varphi_E \end{cases}\end{aligned} \quad \text{(S31)}$$

There is a minimum value of φ_E below which there can be no growth: $\varphi_{E,min} = k'_d/(\kappa_E Y_b)$. Note that if $k'_d = 0$ (i.e: the chitinases never detach) then $\lambda > 0$ and there is no threshold behavior: the culture can always grow. In simpler terms, if enzymes remain on particles and actively produce nutrients, a growing steady-state can always be obtained.

While the overall growth rate $\lambda(\varphi_E)$ shows no k_d dependence, the replication rate of cells on particles, r_s, on the other hand varies with the detachment rate, k_d since $r_s = \lambda + k_d$. Given the form of r_s from Scott et. al (2010) described in Eq. S9, there will be a maximum r_s achieved after which the dominating term will come from chitinase overexpression. To see this, we translate the result for λ in Eq. S31 to r_s and the nutrient concentration n/K. Given Eq. S9:

$$r_s = r_{max}\frac{n/K}{1 + n/K}\left(1 - \frac{\varphi_E}{\varphi_{max}}\right)$$

$$\to \frac{n}{K} = \frac{\lambda + k_d}{r_{max}}\left((1 - \varphi_E/\varphi_{max}) - \frac{\lambda + k_d}{r_{max}}\right)^{-1} \quad \text{(S32)}$$

Let $\frac{n^*}{K}$ be the value at which Eq. S32 diverges. This corresponds to $\varphi_E^* = \varphi_{max}(1 - (\lambda + k_d)/r\_max)$. Therefore:

$$r_s(\varphi_E, k_d) = \begin{cases} \lambda(\varphi_E) + k_d & \text{for } \varphi_E < \varphi_E^* \\ r_{max}\left(1 - \frac{\varphi_E}{\varphi_{max}}\right) & \text{for } \varphi_E > \varphi_E^* \end{cases} \quad \text{(S33)}$$

Similarly, for λ we have:

$$\lambda(\varphi_E, k_d) = \begin{cases} k_E Y_b \varphi_E - k'_d & \text{for } \varphi_E < \varphi_E^* \\ r_{max}\left(1 - \frac{\varphi_E}{\varphi_{max}}\right) - k_d & \text{for } \varphi_E > \varphi_E^* \end{cases} \quad \text{(S34)}$$

9

In principle, the population could increase its chitinase excretion rate until it reaches φ_E^*. However, for the range of parameters we experimentally observe, we find that φ_E is kept rather small by the cells. Specifically, $\varphi_E^* \approx 15\%$ while the measured value of $\varphi_E \approx 3\%$. We speculate that this may be a mechanism to keep nutrient levels $\frac{n}{K}$ low which would result in a tradeoff between k_d and λ. For a fixed nutrient concentration n/K keeping φ_E constant, we find this tradeoff as:

$$\rightarrow \lambda + k_d = r_{max}\left(1 - \frac{\varphi_E}{\varphi_{max}}\right)\frac{n/K}{1+n/K} \tag{S35}$$

c- *An easier derivation*

In this section, we focus on the flux balance between nutrient generation and uptake by replicating cells. Our goal is to give a more intuitive derivation for $\lambda(\varphi_E)$ in the regime in which $\varphi_E < \varphi_E^*$.

The fraction of the total nutrient flux allocated to chitinase synthesis in steady-state is $\varphi_E = J_E/J_n$, where $J_E Y_b = \lambda(\varepsilon_b + \varepsilon_s)$. We rearrange this equation to get $\lambda(\varphi_E)$:

$$\lambda = (\varphi_E J_n Y_b)/(\varepsilon_b + \varepsilon_s) \tag{S36}$$

Eq. S19 allows to explicitly express the total nutrient flux J_n in terms of the other parameters:

$$\lambda = \varphi_E k_E Y_b \left(\varepsilon_s/(\varepsilon_b + \varepsilon_s)\right) \tag{S37}$$

The population increase rate λ only depends on enzyme amounts and not cellular parameters. In particular, it is independent of the detachment rate k_d. Intuitively, this is the simple statement that the rate at which the total population increases only depends on nutrient generation by chitinases regardless of the population partioning between the planktonic and surface asscoiated phase. The ratio $\eta' \equiv \varepsilon_b/\varepsilon_s = k_d'/(\lambda + k_a')$ is determined by Eq. S17, and allows to rewrite λ as:

$$\lambda = \varphi_E k_E Y_b (\lambda + k_a')/(\lambda + k_a' + k_d') \tag{S38}$$

We clearly see that if $k_a' = 0$, we recover the previous result Eq. S34:

$$\lambda + k_d' = \varphi_E k_E Y_b \tag{S39}$$

In the most general case where $k_a' \neq 0$, we can solve the quadratic equation S38 and recover the general result in Eq. S29.

Given the enzyme dynamics in this broadcast case are decoupled from cellular dynamics, this offers an intuitive reason as to why λ is independent of k_d. The linear form of the dependence is akin to the ribosomal growth law observed in many organisms. It states that if the main bottleneck in growth is nutrient production, then the extent of

chitinase secretion determines the growth rate, since it is responsible for dialing nutrient production.

Moreover, the independence of λ from k_d suggests a surprising result: that the system can get away with arbitrarily high detachment rates as long as it's secreting chitinases. This independence of the growth rate from the detachment rate is enabled by the feedback on the surface of the particles between the replication rate of cells and their detachment rate. Fewer cells on particles due to a high detachment rate implies that the nutrient concentration per cell is increased thus resulting in a higher replication rate on the particles. This feedback, facilitated by chitinase secretion and accumulation on the particles stabilizes the system.

d- Some key takeaways:
- A minimum chitinase production amount is required to overcome the detachment of chitinases k_d' and for a steady-state to be possible. This threshold for growth is $\varphi_{E,min} = k_d'/(\kappa_E\,Y_b\,)$
- The overall population increase rate λ depends linearly on φ_E, the allocation towards chitinase production, until $\varphi_E = \varphi_E^*$. At this point, protein overproduction becomes costly, as the nutrient concentration is above what's needed to attain the maximum growth rate r_{max}.
- For a fixed value of φ_E, λ is independent of k_d for $\varphi_E < \varphi_E^*$. This is because in the case of broadcast enzymes, the enzymes' dynamics are decoupled from the cells' dynamics. For $\varphi_E > \varphi_E^*$ it decreases linearly with the detachment rate, k_d.
- For a fixed value of k_d, λ increases linearly with φ_E until it reaches its peak value at $\varphi_E = \varphi_E^*$. After this point, the cost of protein overproduction causes λ to decrease linearly with φ_E.
- Increasing chitinase production such that $\varphi_E = \varphi_E^*$ comes with the disadvantage of increasing the nutrient concentration on the surface of particles, since φ_E^* is defined as the chitinase production level at which the nutrient concentration n/K diverges.

3- **Case of cell-bound enzymes**

a- Constraints on the parameters

To outline the benefits of chitinase excretion uncovered in the previous section, we use our general framework to explore the case in which chitinases remain bound to the cell wall as a contrasting scenario. This means that the enzymes' detachment and attachment rates correspond to those of the cells and that the enzyme production rate is the same as the surface-associated cells' replication rate:

$$k_a' = \ k_a = 0\ ,\ k_d' = k_d \text{ and } \beta_s = r_s^{bound} \qquad\qquad \text{(S40)}$$

Given these constraints on the parameters, we rewrite the general population level model in Eqs. S1-S5 including the experimental findings described in Section 2-a as:

$$\frac{d\rho_b}{dt} = k_d\,\rho_s \tag{S41}$$

$$\frac{d\rho_s}{dt} = (r_s^{bound} - k_d)\rho_s \tag{S42}$$

$$\frac{d\varepsilon_b}{dt} = k_d\,\varepsilon_s \tag{S43}$$

$$\frac{d\varepsilon_s}{dt} = r_s^{bound}\rho_s - k_d\,\varepsilon_s \tag{S44}$$

$$\frac{dn}{dt} = k_E\varepsilon_s - \mu\rho_s \tag{S45}$$

In this case, we see that the equations for ε_i are redundant. Their dynamics are related to those of the ρ_i by a simple ratio. Moreover, we can easily solve this system since all of the variables depend on the dynamics of ρ_s only, which can in turn be trivially solved. In steady-state our model reduces to the following set of equations written in terms of λ^{bound}, the exponential growth rate:

$$\eta \equiv \rho_b/\rho_s = k_d/\lambda^{bound} \tag{S46}$$

$$\lambda^{bound} = r_s^{bound} - k_d \tag{S47}$$

$$\eta' \equiv \varepsilon_b/\varepsilon_s = k_d/\lambda^{bound} = \eta \tag{S48}$$

$$\varepsilon_s/\rho_s = (r_s^{bound})/(\lambda^{bound} + k_d) \tag{S49}$$

$$k_E\varepsilon_s = \mu\rho_s = J_n \tag{S50}$$

b- <u>*Examining the effect of φ_E^{bound} and k_d on the system*</u>

We first examine the effect of the detachment rate k_d on the overall population increase rate λ^{bound} and replication rate r_s. Let us denote the allocation towards chitinase synthesis in this case as φ_E^{bound}.

In steady-state, the flux dedicated to chitinase synthesis $J_E = \varphi_E^{bound}J_n = \varphi_E^{bound}k_E\varepsilon_s$ is:

$$J_E Y_b = \Sigma_i\dot{\varepsilon}_i$$
$$= r_s^{bound}\rho_s \tag{S51}$$

This leads to the simple relation between the replication rate r_s and the allocation towards chitinase synthesis:

$$r_s^{bound} = \varphi_E^{bound}k_E Y_b\varepsilon_s/\rho_s \tag{S52}$$

Substituting this expression for the replication rate in Eq. S47, we get:

$$\lambda^{bound}\left(\varphi_E^{bound}, k_d\right) = k_E Y_b\varphi_E^{bound} - k_d \tag{S53}$$

And thus

$$r_s^{bound}\left(\varphi_E^{bound}\right) = k_E Y_b\varphi_E^{bound} \tag{S54}$$

Including the effect of chitinase overproduction through Eq. S9, allows to find:

$$r_s^{bound} = r_{max} \left(\frac{n/K}{1 + n/K} \right) \left(1 - \varphi_E^{bound}/\varphi_{max} \right)$$

Solving for the nutrient concentration n/K, we find:

$$\rightarrow n/K = \left(\frac{r_{max}}{r_s} \left(1 - \varphi_E^{bound}/\varphi_{max} \right) - 1 \right)^{-1} \tag{S55}$$

Substituting for the value of the replication rate in Eq. S52, the nutrient concentration in this expression diverges when:

$$\varphi_E^{*bound} = \left(k_E Y_b/r_{max} + 1/\varphi_{max} \right)^{-1}$$

The full form solution for the replication rate r_s is thus:

$$r_s^{bound}\left(\varphi_E^{bound}, k_d\right) = \begin{cases} \varphi_E^{bound} k_E Y_b & \text{for } \varphi_E^{bound} < \varphi_E^{*bound} \\ r_{max} \left(1 - \frac{\varphi_E^{bound}}{\varphi_{max}} \right) & \text{for } \varphi_E^{bound} > \varphi_E^{*bound} \end{cases} \tag{S56}$$

The overall population replication rate is:

$$\lambda^{bound}(\phi_E, k_d) = \begin{cases} \varphi_E^{bound} k_E Y_b - k_d & \text{for } \varphi_E^{bound} < \varphi_E^{*bound} \\ r_{max} \left(1 - \frac{\varphi_E^{bound}}{\varphi_{max}} \right) - k_d & \text{for } \varphi_E^{bound} > \varphi_E^{*bound} \end{cases} \tag{S57}$$

c- Comparison between the broadcast and cell-attached case
• In both cases, there is a threshold value of chitinase expression below which no exponential growth can occur. In the case of secreted enzymes, this threshold depends on the chitinases' detachment rate k_d', while in the case of bound enzymes it depends on the cell detachment rate k_d.

• The experimental observation that $k_d/k_d' \approx 10$ illustrates the added difficulty of achieving exponential growth when enzymes remain cell-bound.

• We note that for the same level of chitinase expression $\varphi_E^{bound} = \varphi_E$, the exponential growth rate in the case of secreted enzymes is always higher, such that: $\lambda \geq \lambda_s^{bound}$. The two rates are equivalent if there is no detachment rate.

• Overall, enzyme secretion allows for higher detachment rates of the cells without affecting the overall growth rate.

4- <u>A conflict between privatization and high detachment</u>
Our experimental observations demonstrate that the chitin expression level is kept low $\varphi_E \approx 3\%$. A possible rationale against increasing this level further is that it would lead to higher concentrations of labile nutrients (GlcNAc) on the particle surface (Fig. 4d), which

could in turn promote the growth of cheaters since chitin particles are complex ecological systems[6–9]. Thus, maximizing the population increase rate may not advantage 1A01's long-term survival strategy.

Why don't cells thus "privatize" their resources as a way of bypassing cheaters who may feast on these "public goods"[10,11] by binding them to the cell surface[12–15] such that nutrients generated are immediately taken up? The model outlined above in section 3 examines this scenario (Fig. N-I).

In this case, the observed chitinase expression for 1A01 ($\varphi_E \approx 3\%$) would give rise to a replication rate of $r_s^{bound} \approx 0.06\ h^{-1}$, well below the detachment rate observed $k_d \approx 0.2\ h^{-1}$, thus failing to result in exponential growth. Generally, the overall population increase rate in the case of bound-enzymes (Fig. N-I b) is always lower than in the case of broadcast enzymes (Fig. N-I c).

The physiological reason cells with bound enzymes would experience slower rates in their population increase is that when they detach from particles, these cells carry their bound enzymes with them (Fig. 5a). Since chitinases are only useful when in contact with their substrate, this is a wasteful strategy. In contrast, when enzymes are secreted and released, they remain on particles even as cells detach[16]. This illustrates a basic conflict between binding enzymes to cells and achieving high detachment rates.

To reach a comparable growth rate as 1A01 (red dotted line in Fig. N-I b), cells with bound chitinases would need to increase the allocation for chitinase expression 4-fold, to $\varphi_E \approx 12\%$ of the nutrient influx. This corresponds to ~20% of the cellular proteome on particles (Extended Data Table 1), making it comparable to the entire ribosome content of the cell (Fig. 4f). Such high chitinase expression would deprive cells from expressing a variety of other proteins, e.g., motility, Type-VI secretion system, etc. (Table S1), which can enable the adoption of alternative survival strategies[17].

5- **On the attachment rate**

While our experiments suggest that in the steady-state, the attachment rate $k_a \ll \lambda$, the initial dynamics of the system must rely on an attachment rate that's high enough to get the culture started. Our experiment in Fig.1d where planktonic cells are re-incubated in a fresh culture with fresh chitin particles is surprising in this sense, since we observe no lag time. Is this lack of lag time consistent with our estimate for the attachment rate?

We first provide an order of magnitude estimate for the lag based on the attachment rate. Assuming encounters between cells and particles are diffusion-limited, then the rate Γ for a cell to encounter a particle of radius R_0 is given by

$$\Gamma = 4\pi D_\rho R_0 \rho_c$$

where D_ρ is the effective diffusion coefficient of randomly tumbling 1A01 cells and ρ_c is the particle density. For our experimental samples of chitin cultures, $R_0 \approx 150\ \mu m$ and $\rho_c \approx 3000/mL$. Also, $D_\rho \approx 100\ \mu m^2/s$ based on our measurement of 1A01's swimming characteristics. These numbers lead to an encounter rate of $\Gamma \approx 2/h$. The attachment rate k_a is given by

$$k_a = s \cdot \Gamma$$

where s is the "stickiness", i.e., the probability that a cell attaches to the particle after encounter. The value of this parameter in the literature range between $1 - 10\%$ [18,19].

14

Assuming the stickiness s for 1A01 is on the low end, i.e., $s = 1\%$, then $k_a \approx 0.02/h$ which is barely consistent with the condition $k_a \ll \lambda$.

Next, we note that during the initial stage after inoculation, the dominant process is attachment. If we discard the effect of both growth and detachment, the surface-associated density is:

$$\rho_s(t) = \rho_b(0)(1 - e^{-k_a t})$$

For 10% of the initial population to adhere to the particles given the above parameters, it would take:

$$t^* \approx 5h$$

which is faster than the 12h timescale for the growth of our culture and therefore not easily noticeable in the data of Fig. 1b.

However, if it turns out that $s \ll 1\%$, then $t^* \gg 5h$, and a lag should be readily noticeable.

Experimentally, we can think of a number of practical effects making it difficult to observe a significant lag upon re-incubation of the planktonic component of the chitin culture into fresh chitin media (Fig. 1b):

1- Planktonic cells produce some amount of chitinases which help get the culture started since we observe a small amount of chitinases in their proteome (Table S1).
2- Some small particles containing growing particle-associated cells (which were impossible to exclude completely) were transferred to the fresh chitin culture and they presented an immediate source of growth.
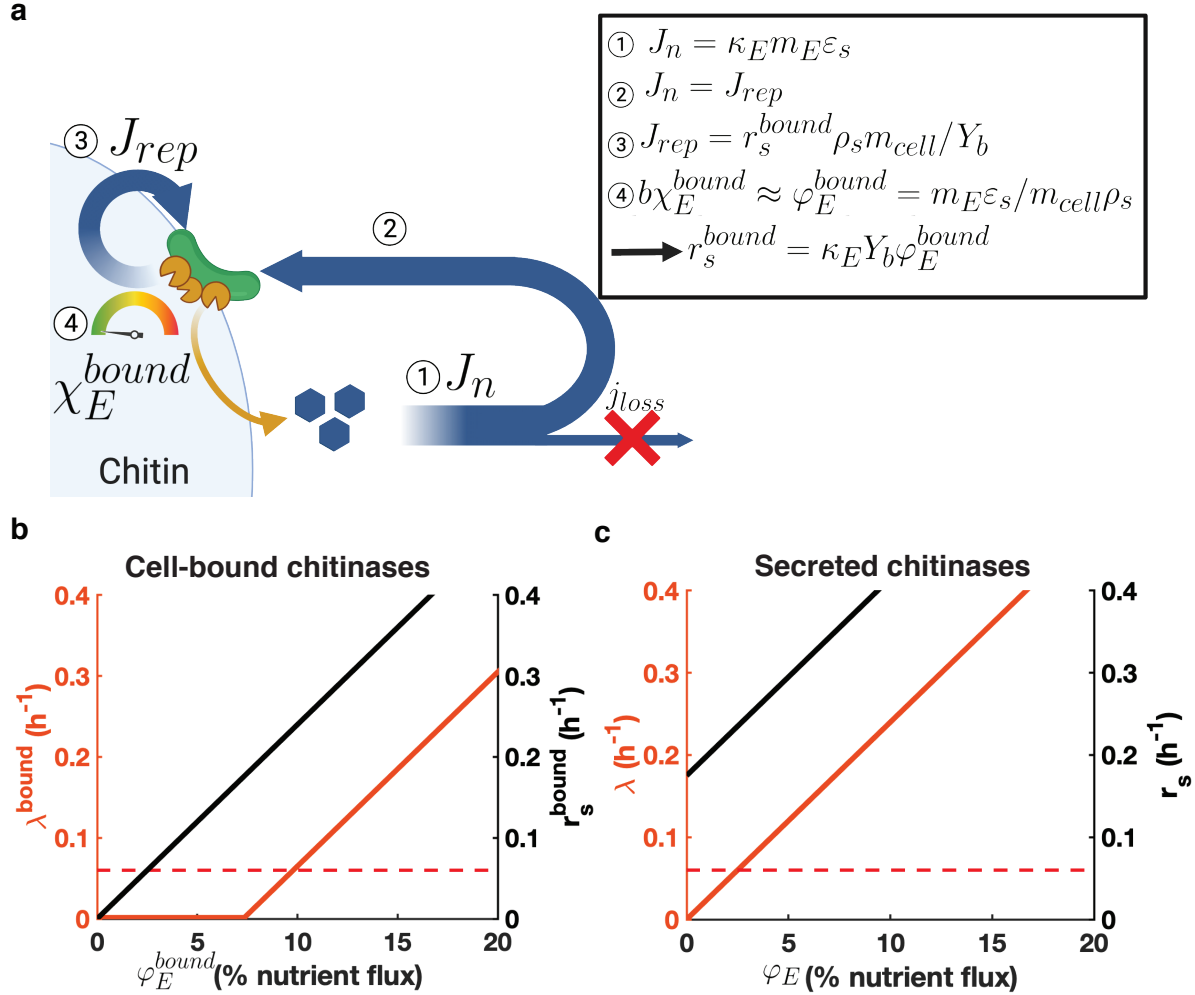
a

$$① \quad J_n = \kappa_E m_E \varepsilon_s$$

$$② \quad J_n = J_{rep}$$

$$③ \quad J_{rep} = r_s^{bound} \rho_s m_{cell}/Y_b$$

$$④ \quad b\chi_E^{bound} \approx \varphi_E^{bound} = m_E \varepsilon_s/m_{cell}\rho_s$$

$$\longrightarrow \quad r_s^{bound} = \kappa_E Y_b \varphi_E^{bound}$$

③ J_{rep}

②

④ χ_E^{bound}

Chitin

① J_n

j_{loss}

b Cell-bound chitinases

λ^{bound} (h^{-1})

r_s^{bound} (h^{-1})

φ_E^{bound} (% nutrient flux)

c Secreted chitinases

λ (h^{-1})

r_s (h^{-1})

φ_E (% nutrient flux)

Figure N-I: The case of enzymes bound to the cell surface. a) Model describing chitinase synthesis and labile nutrient generation by chitinases which are bound to the cell surface. ① Enzymes bound to the surface of the particles, of concentration ε_s (yellow pacmans), produce GlcNAc molecules (blue hexagons) at a rate $m_E \kappa_E \varepsilon_s$, where κ_E is the catalytic rate of the chitinases per enzyme mass and m_E the enzyme mass. ② The total flux of generated nutrients J_n fully goes towards cellular biomass production J_{rep} since the loss of nutrients due to diffusion j_{loss} is negligible during steady state growth; see text. ③ The nutrient flux related to growth is proportional to the replication rate of the cells such that $J_{rep} = r_s^{bound} \rho_s m_{cell}/Y_b$ where r_s^{bound} is the replication rate of surface associated cells, ρ_s their density and the factor m_{cell}/Y_b simply a conversion factor between biomass and nutrient concentration. ④ The fraction of the total flux J_n allocated towards chitinase synthesis is χ_E^{bound} and can be dialed by the cells. It can be expressed as $b\chi_E^{bound} = \varphi_E^{bound} \approx m_E \varepsilon_s/m_{cell}\rho_s$ where $b = m_p/m_{cell}$. Taken together, relations ① through ④ lead to the equation describing the replication rate of surface associated cells Eq. (8) $r_s^{bound} = \kappa_E Y_b \varphi_E^{bound}$. **b)** Growth rate λ^{bound} (left, red axis) and replication rate of surface associated cells r_s^{bound} as a function of the chitinase fraction χ_E^{bound} in the case of cell-bound

16

enzymes for the measured detachment rate, $k_d = 0.18h^{-1}$. In this case, it is the replication rate that is proportional to the chitinase fraction whereas the overall population increase rate is reduced by the detachment rate. We see that at the chitinase level measured for 1A01 $\varphi_E = 3\%$, the system cannot achieve an exponentially increasing steady-state. To achieve a similar population increase rate than 1A01, $\lambda^{bound} = 0.06h^{-1}$ (indicated by the dotted red line), cells would need to express ~3 times as many chitinases $\varphi_E^{bound} \approx 10\%$. **c)** As a comparison, we once again plot the growth rate (left, red axis) and replication rate (right black axis) for the case of secreted enzymes as a function of chitinase expression for the measured detachment rate $k_d = 0.18h^{-1}$. The red dotted line corresponds to the observed growth rate $\lambda = 0.06h^{-1}$. Comparing Panels b and c, we see that for a similar chitinase expression level where $\varphi_E^{bound} = \varphi_E$, λ^{bound} is always lower than λ.

II-On chitinase dynamics

In this section we explain how the parameters governing chitinase dynamics (Figs. 4 and Extended Data Fig.6 in the main text) were determined. Experiments consisted of extracting samples from a steady-state growing culture at different planktonic ODs. These samples were then treated with chloroform to disable nutrient uptake by the cells, which allowed to directly monitor the production of nutrients. Control experiments showed that chloroform indeed disabled cell growth and GlcNAc uptake but that it had a detrimental effect on the activity of purified enzymes. This effect is taken into account for assessing the catalytic rate of the enzymes (see Methods).

We measured GlcNAc concentration accumulation traces over time given an initial planktonic OD. To interpret this data, we used a simple model in which two pools of enzymes, planktonic enzymes ε_b and enzymes attached to the surface of the particles ε_s can attach and detach with rates k_a' and k_d' . Only enzymes attached to the surface of the particles can produce nutrients with a catalytic rate k_E.

This corresponds to Eqs. S1-S5 in the case where $\rho_b = \rho_s = 0$:

$$\frac{d\varepsilon_b}{dt} = k_d'\varepsilon_s - k_a'\varepsilon_b \tag{S58}$$

$$\frac{d\varepsilon_s}{dt} = k_a'\varepsilon_b - k_d'\varepsilon_s \tag{S59}$$

$$\frac{dn}{dt} = k_E\varepsilon_s \tag{S60}$$

Our goal is to solve for the full dynamics of $n(t)$. Let $\varepsilon_{tot} = \varepsilon_b + \varepsilon_s$ be the total amount of chitinases in the system:

$$\frac{d\varepsilon_{tot}}{dt} = \frac{d\varepsilon_b}{dt} + \frac{\varepsilon_s}{dt} = 0 \tag{S61}$$

The conservation of ε_{tot} allows to reduce the system in terms of one variable only:

$$\frac{d\varepsilon_s}{dt} = k_d'(\varepsilon_{tot} - \varepsilon_s) - k_d'\varepsilon_s \tag{S62}$$

$$\frac{dn}{dt} = k_E\varepsilon_s \tag{S63}$$

Eq. S62 can be easily solved given the initial condition $\varepsilon_s(0)$:

$$\varepsilon_s(t) = \frac{k_{a'}\varepsilon_{tot}}{k_{a'}+k_{d'}} + \left(\varepsilon_s(0) - \frac{k_{a'}\varepsilon_{tot}}{k_{a'}+k_{d'}}\right)e^{-(k_a'+k_d')t} \tag{S64}$$

We then integrate Eq. S64 to find the solution of Eq. S63 given the initial condition $n(0) = 0$ to find:

$$\frac{n(t)}{k_E} = \frac{k_{a'}\varepsilon_{tot}}{k_{a'}+k_{d'}}t - \left(\frac{\varepsilon_s(0)}{k_{a'}+k_{d'}} - \frac{k_{a'}\varepsilon_{tot}}{(k_{a'}+k_{d'})^2}\right)\left(e^{-(k_a'+k_d')t} - 1\right) \tag{S65}$$

Let us consider various limits of Eq. S65. At short times, (i.e: $t \ll \frac{1}{k_{a\prime}+k_{d\prime}}$):

$$\lim_{t \to 0} \frac{n(t)}{k_E} = \frac{k_{a\prime}\varepsilon_{tot}}{k_{a\prime}+k_{d\prime}}t + \left(\frac{\varepsilon_s(0)}{k_{a\prime}+k_{d\prime}} - \frac{k_{a\prime}\varepsilon_{tot}}{(k_{a\prime}+k_{d\prime})^2}\right)(k_a' + k_d')t$$
$$= \varepsilon_s(0)t \qquad\qquad \text{(S66)}$$

Initially, the GlcNAc concentration increases linearly with a slope $s_1 = k_E\varepsilon_s(0)$, allowing to estimate the value of k_E.

At longer times, (i.e: $t \gg \frac{1}{k_{a\prime}+k_{d\prime}}$):

$$\lim_{t \to \infty} \frac{n(t)}{k_E} = \frac{k_{a\prime}\varepsilon_{tot}}{k_{a\prime}+k_{d\prime}}t + \left(\frac{\varepsilon_s(0)}{k_a'+k_d'} - \frac{k_a'\varepsilon_{tot}}{(k_a'+k_d')^2}\right) \qquad\qquad \text{(S67)}$$

The GlcNAc concentration increases linearly with a slope $s_2 = k_E \frac{k_a'\varepsilon_{tot}}{k_a'+k_d'}$. Taking the ratio of the two slopes allows us to determine the ratio k_d'/k_a' since:

$$\frac{s_1}{s_2} = \varepsilon_s(0)/\varepsilon_{tot}(1 + k_d'/k_a') \qquad\qquad \text{(S68)}$$

The time scale at which $n(t)$ changes from one slope to the other allows to fix $k_a' + k_d'$ and determine all parameters. We notice that the two lines described in Eqs. S66 and S67 intersect exactly at $t^* = 1/(k_a' + k_d')$

$$\varepsilon_s(0)t^* = \frac{k_a'\varepsilon_{tot}}{k_a' + k_d'}t^* + \left(\frac{\varepsilon_s(0)}{k_a' + k_d'} - \frac{k_a'\varepsilon_{tot}}{(k_a' + k_d')^2}\right)$$
$$\to t^* = (k_a' + k_d')^{-1} \qquad\qquad \text{(S69)}$$

Given the estimates for $\varepsilon_s(0)$ and ε_{tot}, we determine the value of the enzyme parameters k_a', k_d' and k_E.

III- Spatial model for growth on a chitin particle

A key assumption made in our population-level model (Supp. I) is that the flux of nutrients is balanced: all nutrients generated are used for either biomass or chitinase production and none are lost to the surrounding environment. This assumption which was backed by our data (Fig. 2, ED Figs. 2,3) allowed us to collapse the spatial structure into a simple two-compartment model: planktonic vs. particle-associated cells and enzymes.

Theoretically, this assumption is justified because nutrient generation, which is proportional to the chitinase concentration on particles, and the nutrient uptake, which is proportional to the number of cells on particles, are both increasing exponentially, whereas the nutrient leakage is finite (because the nutrient concentration on the surface does not increase with time). Therefore, in the long-time limit, nutrient leakage will be an exponentially small fraction of the flux of nutrient generation and uptake.

Below, we provide a simplified spatial model to see how this balance quantitatively works out. In the more realistic case, cell colonies on the particles may be patchy (ED Fig.4) and these patches may not be co-localized with the enzymes. However, such mismatches are unlikely to last long since cells would chemotax to the vicinity of nutrients [20] and they will then replicate more rapidly until the local nutrient generation and uptake fluxes are balanced.

1- <u>Case with a constant planktonic cell density</u>

Let us consider a spherical chitin particle of radius R_0 coated with a monolayer of cells at the surface with density σ. A similar model is developed in Nguyen et al. (2021)[21]. GlcNAc is generated at the surface with a rate $k_E \varepsilon_s$ where k_E is the catalytic rate of the enzymes as determined above and ε_s is the active enzyme concentration on the surface of the particles. Away from the particles, let's consider planktonic cells with uniform density ρ_b.

Both surface associated and planktonic cells uptake nutrients following Monod kinetics with growth rate $r(n(R)) = \frac{r_{max} n(R)}{K_n Y}$ where R is their radial position away from the center of the particle and Y is the yield of 1A01 cells growing on GlcNAc monomers.

From this formulation, it is clear that the nutrient gradient determines the replication rates of the two cellular subpopulations. The nutrient concentration in the system is:

$$\frac{\partial n(R,t)}{\partial t} = D_n \nabla^2 n(R,t) + k_E \varepsilon_s(t)\delta(R - R_0) - \frac{r_{max} n(R_0, t)}{K_n Y}\sigma(t)\delta(R - R_0)$$
$$- \frac{r_{max} n(R,t)}{KY}\rho_b(t)\Theta(R - R_0) \qquad (S70)$$

where δ is the Dirac delta function and Θ is the Heaviside step function.

By assuming instantaneous equilibration of the nutrient field (i.e: $\frac{\partial n(R,t)}{\partial t} = 0$), writing the Laplacian in spherical coordinates as $\nabla^2 n(R) = \frac{1}{R}\frac{d^2}{dR^2}(R \cdot n(R))$ and defining $g(R) = R \cdot n(R)$, we solve the following equation for the nutrient field:

$$D_n g''(R) + R k_E \varepsilon_s \delta(R - R_0) - \frac{r_{max} g(R_0)}{K_n Y} \sigma \delta(R - R_0)$$
$$- \frac{r_{max} g(R)}{K_n Y} \rho_b \Theta(R - R_0) = 0 \qquad \text{(S71)}$$

For the region $R > R_0$, this simplifies to:

$$g''(R) = \frac{r_{max} \rho_b}{D_n K_n Y} g(R) = \kappa^2 g(R) \qquad \text{(S72)}$$

Where we define $\kappa^2 = \frac{r_{max} \rho_b}{D_n K_n Y}$ such that κ^{-1} is the screening length.

The boundary condition at R_0 is found by integrating Eq. S71 in an infinitesimal region around R_0:

$$D_n(g'(R_0^+) - g'(R_0^-)) + R_0 k_E \varepsilon_s - \frac{r_{max} g(R_0)}{K_n Y} \sigma$$
$$- \frac{r_{max}}{K_n Y} \rho_b (g(R_0^+) - g(R_0^-)) = 0 \qquad \text{(S73)}$$

To prevent inward diffusive flux we have that $g'(R_0^-) = n_0$, and $g(R_0^+) = g(R_0^-)$ to insure continuity. Simplifying the above equation, we get:

$$D_n g'(R_0) - D_n n_0 + R_0 k_E \varepsilon_s - \frac{r_{max} g(R_0)}{K_n Y} \sigma = 0 \qquad \text{(S74)}$$

$$g'(R_0) - n_0 + \frac{R_0}{D_n} k_E \varepsilon_s - \frac{r_{max} g(R_0)}{D_n K_n Y} \sigma = 0 \qquad \text{(S75)}$$

The solution to Eq. S74 where $g(R \to \infty)$ is bounded is:

$$g(R) = g_0 e^{-\kappa(R - R_0)} \qquad \text{(S76)}$$

In terms of the nutrient concentration explicitly:

$$n(R) = \frac{n_0 R_0}{R} e^{-\kappa(R - R_0)} \qquad \text{(S77)}$$

Where n_0 is obtained by solving the boundary condition

$$n_0 = \frac{k_E \varepsilon_s}{D_n(\kappa + R_0^{-1}) + \frac{r_{max}}{K_n Y}\sigma} \qquad \text{(S78)}$$

Note that for $\kappa^{-1} \gg R_0$ we have $n_0 = \frac{R_0 k_E \varepsilon_s}{D_n(1 + \frac{r_{max}}{K_n Y}\sigma)}$ and for $\kappa^{-1} \ll R_0, n_0 = \frac{k_E \varepsilon_s}{\kappa D_n}$

In our experiment, $R_0 \approx 150\mu m$ and the chitin weight density, $\phi_w = 0.2\% w/v$. Given the density of chitin $d_c = 1.4 \ g/cm^3$, we estimate the volume density of chitin particles as

$\phi_v = \phi_w/d_c = 1.4 \times 10^{-3}$. This allows to infer the inter-particle spacing $\ell_c = R_0/\phi_v^{1/3} \approx$ $9R_0$. Moreover, the cell surface density is $\sigma = \left(\frac{\eta R_0}{3\phi_v}\right)\rho_b$ where $\eta = \rho_b/\rho_s$.

The parameters in Table N-III allow us to estimate the screening length: $29\mu m <$ $\kappa^{-1} < 94\mu m$. This is of the order of the particle size, but 10 times smaller than the inter-particle spacing, l. We also estimate the value of n_0, the nutrient concentration on the surface of chitin particles as $5\ \mu M < n_0 < 20\ \mu M$. This strongly suggests that beyond the small screening distance determined by κ^{-1}, there is no planktonic replication in the bulk as the nutrient concentration $n(R)$ would quickly fall below the Monod constant, K_n, which we take to be $\sim 1\ \mu M$.

Parameter	Symbol	Estimated value
Maximum growth rate	r_{max}	$0.8h^{-1}$
Yield on GlcNAc	Y^{-1}	$6.1\ mM/OD_{600}^{plank}$
Monod constant for GlcNAc	K_n	$1\ \mu M$
Diffusion coefficient of GlcNAc	D_n	$600\ \mu m^2/s$
Diffusion coefficient of cells	D_ρ	$100\ \mu m^2/s$
Planktonic density in the culture	ρ_b	$0.05 - 0.5\ OD_{600}^{plank}$
Interparticle spacing	ℓ_c	$1.5\ mm$

Table N-III: Parameters for spatial model of chitin degradation

2- **Case with a spatially-dependent planktonic cell density**

An important approximation made in the model described above was the constancy of the planktonic cell density. Let us now relax that assumption and allow this cellular field to have spatial structure in response to the spatial nutrient profile. We will analyze the effect of the spatial nutrient profile on the spatial cell density profile and thus reexamine the validity of the constant cell density approximation made above.

Let $\rho(R, t)$ be the planktonic cell density profile. The random tumbling motion of planktonic cells can be effectively described by diffusion at the population level, with a diffusion constant D_ρ, while chemotaxis towards nutrients (which can also be chemoattractant[20]) can be described by a concentration-dependent convection term to be detailed below. Additionally, those cells close to the particle can replicate, at a rate that depends on the local nutrient concentration through a Monod form and a Monod constant K_n. Similarly to the model above, let $n(R, t)$ be the nutrient profile which diffuses with a constant D_n and is consumed by both planktonic and surface-associated cells. Again, nutrients are produced on the surface of the particles with a rate $k_E \varepsilon_s(t)$. Our system is now comprised of this set of two coupled differential equations:

$$\frac{\partial n(R,t)}{\partial t} = D_n \nabla^2 n(R,t) + \left(k_E \varepsilon_s(t) - \frac{r_{max} n(R_0,t)}{K_n Y} \sigma(t) \right) \delta(R - R_0)$$

$$- \frac{r_{max} n(R,t)}{K_n Y} \rho(R,t) \Theta(R - R_0) \tag{S80}$$

$$\frac{\partial \rho(R,t)}{\partial t} = D_\rho \nabla^2 \rho(R,t) + r_{max} \frac{n(R,t)}{n(R,t) + K_n} \rho(R,t)$$

$$- \chi \nabla \left(\frac{\nabla n(R,t)}{n(R,t) + K_\chi} \rho(R,t) \right) \tag{S81}$$

We note that in the last term on the right-hand side of Eq. S81, we describe chemotaxis by a modified log-sensing form (or Weber's law, $\nabla n(R,t)/n(R,t)$), with a concentration cutoff K_χ and with χ being the chemotactic coefficient. The role of this cutoff is to capture the limited sensitivity of cells to a very low concentration of chemoattractant [22–25]. It plays a crucial role here since in the singular-limit $K_\chi \to 0$, chemotaxis would guide cells from infinitely far away to the particle, even if the nutrient profile attenuates exponentially away from the particle.

Assuming the nutrient field equilibrates instantaneously, i.e., $\frac{\partial}{\partial t} n(R,t) = 0$ (since this timescale is much faster than changes in the planktonic cell density which increase over the time scale λ^{-1}), Eq. S80 for $R > R_0$ becomes

$$\nabla^2 n(R,t) = \frac{r_{max}}{D_n K_n Y} \rho(R,t) n(R,t), \tag{S82}$$

which is a nonlinear equation with $\rho(R,t)$ obtained from the solution to Eq. S81, another nonlinear equation. To progress further, we assume that the spatial planktonic cell density profile is only weakly dependent on R and can be considered constant within the millimeter length scale of inter-particle spacing. In other words, we assume $\rho(R,t) \approx \rho(R_0,t)$ as will be self-consistently justified below. With this additional assumption, Eq.(S82) can be solved as described above (Eq. (S71)-(S76)), with the solution

$$n(R,t) = n(R_0,t) \frac{R_0}{R} e^{-\kappa_n(t) \cdot (R-R_0)} \propto e^{-\kappa_n(t) \cdot (R-R_0)} \tag{S83}$$

where $\kappa_n(t) = \sqrt{\frac{r_{max}}{D_n K_n Y} \rho(R_0,t)}$ is the inverse length scale characterizing the spatial nutrient profile at time t. Since $\rho(R_0,t)$ increases exponentially with $\rho(R_0,t) = \rho(R_0) e^{\lambda t}$, we see that κ_n^{-1}, the length scale of the nutrient field, gets exponentially smaller, i.e., $\kappa_n^{-1} \sim e^{-\lambda t/2}$. This means that for exponentially growing cells, the nutrient field gets increasingly localized near the surface of the particle. Similarly to above, for the range of cell densities in our experiments, $0.05 < \rho(t) < 0.5$, we find $29\mu m < \kappa_n^{-1} < 94\mu m$. This length scale, which exponentially decreases in time, is at most 6% of the interparticle spacing ($\ell_c = 1.5mm$).

Given this form of κ_n for $n(R,t)$ in Eq. S83, we can ignore both the uptake and chemotaxis term in Eq. S81 for $R \gg \kappa_n^{-1}$. Eq. S81 then becomes:

$$\lambda\rho(R,t) = D_\rho\nabla^2\rho(R,t) \qquad (S84)$$

The solution is

$$\rho(R,t) \propto e^{\kappa_\rho(R-R_0)+\lambda t} \qquad (S85)$$

where $\kappa_\rho^{-1} = \sqrt{D_\rho/\lambda}$. Using parameter values listed in Table N-III, we find $\kappa_\rho^{-1} \sim 2.5\ mm$, which self-consistently justifies the assumption on the weak R-dependence we made above. As this is well above the interparticle spacing in our culture, we conclude that the planktonic cell field is delocalized and can be treated approximately as constant.

Although our analysis suggests that the chemotactic term can be ignored since the nutrient concentration quickly drops below the chemotactic sensitivity K_χ, we note that chemotaxis would affect the macroscopic attachment and detachment rates (the parameters k_a and k_d introduced in the main text Eqs. 1-2). Indeed this term tends to localize cells to the vicinity of the particle and thus affect the repartition of surface-associated and planktonic cells near them, thereby modifying the dependence of k_a and k_d on the microscopic attachment and detachment rates that connect $\rho(R_0,t)$ and the density of cells associated with the surface, $N_s(t)$ via boundary conditions for $\rho(R,t)$.

Another effect of chemotaxis is to increase the chitospheric cell density within the distance κ_n^{-1}. As these cells experience nutrient concentrations similar to that on the particle surface and exchange rapidly with the particle-associated cells, we can regard them together with the cells on particle as "particle-associated" sub-population of cells, referred to as ρ_s in the main text. These modified definitions of k_a, k_d, and ρ_s do not affect the model in the main text which is phenomenological in nature. Detailed solution and analysis of the model defined by Eq. S80, S81, and the accompanying boundary conditions will be presented elsewhere.

SUPPLEMENTARY REFERENCES

1. Amarnath, K. *et al.* Stress-induced cross-feeding of internal metabolites provides a dynamic mechanism of microbial cooperation. 2021.06.24.449802 Preprint at https://doi.org/10.1101/2021.06.24.449802 (2021).

2. Iffland-Stettner, A. *et al.* A Genome-Scale Metabolic Model of Marine Heterotroph Vibrio splendidus sp. 1A01. 29 doi:https://doi.org/10.1101/2022.04.15.488298.

3. Scott, M., Gunderson, C. W., Mateescu, E. M., Zhang, Z. & Hwa, T. Interdependence of Cell Growth and Gene Expression: Origins and Consequences. *Science* **330**, 1099–1102 (2010).

4. You, C. *et al.* Coordination of bacterial proteome with metabolism by cyclic AMP signalling. *Nature* **500**, 301–306 (2013).

5. Hui, S. *et al.* Quantitative proteomic analysis reveals a simple strategy of global resource allocation in bacteria. *Mol. Syst. Biol.* **11**, 784 (2015).

6. Drescher, K., Nadell, C. D., Stone, H. A., Wingreen, N. S. & Bassler, B. L. Solutions to the Public Goods Dilemma in Bacterial Biofilms. *Curr. Biol.* **24**, 50–55 (2014).

7. Pollak, S. *et al.* Public good exploitation in natural bacterioplankton communities. https://www.science.org/doi/10.1126/sciadv.abi4717 doi:10.1126/sciadv.abi4717.

8. Enke, T. N., Leventhal, G. E., Metzger, M., Saavedra, J. T. & Cordero, O. X. Microscale ecology regulates particulate organic matter turnover in model marine microbial communities. *Nat. Commun.* **9**, 2743 (2018).

9. Pontrelli, S. *et al.* Metabolic cross-feeding structures the assembly of polysaccharide degrading communities. *Sci. Adv.* **8**, eabk3076 (2022).

10. Otto, S. B. *et al.* Privatization of Biofilm Matrix in Structurally Heterogeneous Biofilms. *mSystems* **5**, e00425-20 (2020).

11.   Jin, Z. *et al.* Conditional privatization of a public siderophore enables Pseudomonas aeruginosa to resist cheater invasion. *Nat. Commun.* **9**, 1383 (2018).

12.   Meibom, K. L. *et al.* The Vibrio cholerae chitin utilization program. *Proc. Natl. Acad. Sci.* **101**, 2524–2529 (2004).

13.   Itoh, T. *et al.* Cooperative Degradation of Chitin by Extracellular and Cell Surface-Expressed Chitinases from Paenibacillus sp. Strain FPU-7. *Appl. Environ. Microbiol.* **79**, 7482–7490 (2013).

14.   Itoh, T. *et al.* Overexpression, purification, and characterization of Paenibacillus cell surface-expressed chitinase ChiW with two catalytic domains. *Biosci. Biotechnol. Biochem.* **78**, 624–634 (2014).

15.   Itoh, T. *et al.* Crystal Structure of Chitinase ChiW from Paenibacillus sp. str. FPU-7 Reveals a Novel Type of Bacterial Cell-Surface-Expressed Multi-Modular Enzyme Machinery. *PloS One* **11**, e0167310 (2016).

16.   Smith, D. C., Simon, M., Alldredge, A. L. & Azam, F. Intense hydrolytic enzyme activity on marine aggregates and implications for rapid particle dissolution. *Nature* **359**, 139–142 (1992).

17.   Johnson, C. N. Fitness Factors in Vibrios: a Mini-review. *Microb. Ecol.* **65**, 826–851 (2013).

18.   Kiørboe, T., Grossart, H.-P., Ploug, H. & Tang, K. Mechanisms and Rates of Bacterial Colonization of Sinking Aggregates. *Appl. Environ. Microbiol.* **68**, 3996–4006 (2002).

19.   Słomka, J. *et al.* Encounter rates prime interactions between microorganisms. *Interface Focus* **13**, 20220059 (2023).

20.   Bassler, B. L., Gibbons, P. J., Yu, C. & Roseman, S. Chitin utilization by marine bacteria. Chemotaxis to chitin oligosaccharides by Vibrio furnissii. *J. Biol. Chem.* **266**, 24268–24275 (1991).

21.   Nguyen, T. T. H. *et al.* Microbes contribute to setting the ocean carbon flux by altering the fate of sinking particulates. *Nat. Commun.* **13**, 1657 (2022).

22.   Celani, A., Shimizu, T. S. & Vergassola, M. Molecular and Functional Aspects of Bacterial Chemotaxis. *J. Stat. Phys.* **144**, 219–240 (2011).

23.   Shoval, O. *et al.* Fold-change detection and scalar symmetry of sensory input fields. *Proc. Natl. Acad. Sci.* **107**, 15995–16000 (2010).

24.   Tu, Y. Quantitative Modeling of Bacterial Chemotaxis: Signal Amplification and Accurate Adaptation. *Annu. Rev. Biophys.* **42**, 337–359 (2013).

25.   Tu, Y., Shimizu, T. S. & Berg, H. C. Modeling the chemotactic response of Escherichia coli to time-varying stimuli. *Proc. Natl. Acad. Sci.* **105**, 14855–14860 (2008).